ShaneAO Documentation

Release 0

Don Gavel

Mar 15, 2018

CONTENTS

Contents:

ONE

SHANEAO INSTRUMENT DOCUMENT

This document contains a description of the ShaneAO system goals, requirements, and design, and provides the observer's and operator's guides.

Version history

Version	Description	Author	Date
0.1	Initial, according to Documentation Plan	Don Gavel	7/16/2010
0.4	Initial material in the Design Document section	Don Gavel	3/8/2012
0.8	Intermediate edits just before the design review, with pending items highlighted comments	Don Gavel	4/16/2012
1.0	Final edits for design review release	Don Gavel	4/19/2012
1.4	Fixes to cross-references	Don Gavel	4/23/2012
1.5	Converted to restructured text master version, Sphinx doc generators, and maintenance in a Git repository	Don Gavel	9/13/2016

1.1 Introduction

The ShaneAO System is an adaptive optics imager and spectrograph designed for astronomical observations from 650 nm through 2.5 microns wavelength (part of R, and all of I, J, H, and K astronomical bands) using the Shane 3-meter telescope. The system uses adaptive optic technology for correction of atmospheric and telescope aberrations and a high-sensitivity infrared science detector. The imager is sampled at the diffraction-limit for wavelengths longer than 1.0 micron.

This document provides the top-level reference source for documentation of the system requirements and design, along with a guide to operation and maintenance.

The basic instrument capabilities and performance objectives are outlined in this chapter, which consists of material mostly taken from the original proposal to the National Science Foundation (*Gavel and Rockosi 2009*).

1.1.1 Background

The ShaneAO System, which is due to be commissioned in 2013, is an upgrade of the Lick 3-Meter Laser Guidestar AO system. The Lick AO system was installed as an experimental system in 1994 as one of the first astronomical AO systems to use a laser for a wavefront beacon. The AO system was upgraded and outfitted with a new infrared

science camera, IRCAL, in 2000 (*Gavel, et. al., 2000*) and, after refurbishment and automation of the laser, was made available as a facility instrument in 2002. IRCAL used the then new PICNIC array detector, a derivative of the NICMOS effort for Hubble Space Telescope. IRCAL is Nyquist-sampled at K band given the AO corrected beam, is 256x256 pixels covering about 20 arcseconds of science field. Today, the Lick AO system typically delivers a Strehl of 0.3 in K band in laser guidestar observing.

The upgrade introduces a number of improvements that reflect the advances in technology made since 1994 and will provide considerable upgrade in performance as a result. First of all, the AO system will be improved to provide a typical Strehl of 0.3 in I band, opening up the I, J and H as well as K infrared bands to diffraction-limited imaging. Secondly, IRCAL will be retrofitted with a new Hawaii-2RG detector. The new detector has smaller pixels than the PICNIC so it is Nyquist-sampled at the diffraction-limit for $\lambda > 1.0$ μm, and it has more pixels so that it more than adequately covers the original 20 arcsecond science field.

1.1.2 Example Science Uses

Lick Observatory is located at an elevation of 4200 feet atop Mt Hamilton east of San Jose. Time is assigned competitively with astronomers from all of the University of California (UC) 10 campuses and the associated labs (Lawrence Livermore National Lab, Lawrence Berkeley National Lab and the UC Berkeley Space Sciences Lab) eligible to apply. Through collaborations with other astronomers world-wide and including postdocs and graduate students in the UC system, Lick Observatory telescopes are available to a significant fraction of the US astronomical community. As we have completed the infrastructure to allow remote observations at Lick Observatory using stations at most of the UC campuses, the oversubscription rate on the 3-meter telescope is increasing. The site generally enjoys clear weather from May through November with good image quality. The location near to San Francisco Bay area communities has led to increasingly compromised sky brightness in the optical bandpasses, but for $\lambda > 800$nm, the sky at Mt Hamilton is as dark as the best sites in the world.

The 3-meter telescope diffraction limit is $\lambda(\mu m)$ x 0.07". At $\lambda = 1\mu$ this is approximately an order of magnitude higher spatial resolution than delivered by the uncorrected atmosphere at the best ground-based sites. For point sources and background-limited observations (the norm at wavelengths longer than 1μ) the gains in sensitivity scale as the image size squared. There are a large number of science programs that have been built around imaging at this spatial resolution and obtaining spectra in the near-IR with very significantly reduced sky background based on the use of narrower slits in an AO-corrected focal plane. The 3-meter AO system is in regular use and has produced a number of interesting science results. In the Solar System, this resolution is sufficient to determine directly the shapes and rotation axes of asteroids and the incidence of binary asteroid systems (*Marchis et al. 2003*, *Drummond et al. 2008*) and to carry out spatially-resolved studies of the surfaces of planets and the larger moons (e.g. *Roe et al. 2001*). Other studies to date with the 3-meter AO system have been surveys for multiplicity among low-mass stars and stars known to harbor planets (*Patience et al. 2002*, *Marcy et al. 2001*, *Burgasser et al. 2005*), morphological studies of AGN and QSO host galaxies (Lacy et al. 2002, 2006), the environments of ULIRGs (*Laag et al. 2006*) and the centers of late-time galaxy collision remnants (*Bogdanovic et al. 2003*).

The current AO system at Lick Observatory was developed in the early 1990s and, although a pioneer system and state of the art for many years, there are limitations in delivered Strehl. The IR detector in IRCAL, the AO science camera, is several generations old. With the improved capabilities described in this program we believe the already high demand will go even higher and even anticipate some programs now carried out on the Keck system will be moved to the 3-meter.

The improved science reach for the new AO system comes from the increased throughput, higher Strehl and better camera focal plane sampling. All of the current programs will benefit greatly and new programs will now be possible. As discussed elsewhere, the astronomy community that has access to Lick Observatory is large and the science interests very broad. We discuss here a few example science programs, but this is by no means a complete list.

For point sources, the expected sensitivity gain will reduce the time to a reach a given S/N at fixed magnitude by factors of 18, 16 ,11.5 in J,H,K bands. Equivalently, the system brings within reach targets that have correspondingly smaller fluxes. For fixed luminosity limit, as for investigations of binarity fractions in nearby stars as a function of spectral type (e.g., *Goldman et al. 2008*), the increase in sensitivity corresponds to an increase in the available

sample volume by a factor of 8 (H band). For proper motion studies, the sensitivity improvements increase the number of objects available in each field.

Studies of extended sources will also benefit from the upgrade. The improved Strehl will enable morphological classification to fainter magnitudes and of smaller galaxies, and detailed studies of debris disk and other extended features around stars. High Strehl also reduces the background in regions close to bright point sources. Two examples where this latter feature is powerful, discussed in more detail in the following paragraphs, are studies of QSO host galaxies and identification of line-of-sight absorbing systems.

That there is a tight connection between central black holes and the properties of their host galaxies is quantified by correlations like the M_BH-sigma relation (e.g., *Ferrarese & Merritt 2000*, *Gebhardt et al. 2000*). How the black hole controls the evolution of its host galaxy to establish this relation is one of the major open questions of galaxy formation. There are many pieces to understanding where quasars fit in the evolution of galaxies over cosmic time: how the quasar phase is triggered, how the lifetime of the quasar phase relates to the growth rate of the black hole, whether and how energy from BH accretion couples to the gas in the rest of the galaxy to drive the AGN feedback mechanisms invoked by galaxy evolution models, and what observational consequences AGN feedback has for the morphology and star formation rate of their host galaxies. The enormous database of known QSOs from surveys like the SDSS provides a great science opportunity using the improved sensitivity to undertake a systematic study of the properties of host galaxies of QSOs to address these questions.

A related observational problem is identification of the galaxies associated with QSO damped Lyman alpha absorption (DLA) systems. At low redshift (z<1) these systems have been shown (*Chen & Lanzetta 2003*), to be associated with star forming galaxies. The distribution of magnitude and surface brightnesses for the DLA galaxies is not well constrained by existing observations, and the low metalllicity values for low redshift DLAs (*Kulkarni 2004*) suggest that they might be low surface brightness or dwarf galaxies. DLAs are one of our only probes of the interstellar medium in high redshift galaxies, but in order to use that information we need low-redshift observations of the DLA galaxies to relate the gas-phase abundance measurements to luminosity, surface brightness, size and morphology.

Because a DLA line of sight intersects the absorbing galaxy where the baryons are in the disk and bulge, the starlight is likely to be concentrated at small projected distances from the QSO. Contamination from the QSO light raises the background and reduces the detection efficiency. As for the QSO host galaxies, the improvement in Strehl will lower the QSO contamination and enable detection of fainter DLA host galaxies. In a Gemini AO study of DLA systems at z<0.5, *Chun et al. (2006*) find likely candidates for the absorbing systems in all seven of their fields. The galaxies are faint, L < 0.1L*, and have scale lengths <~ 1 kpc. Despite their small sizes, these galaxies are resolved at z<0.5 in diffraction-limited imaging on the 3m, so the detection limits are a function of both surface brightness and total magnitude. We impose a reasonable surface brightness limit at one magnitude fainter in magnitudes arcsec2 than the surface brightness of the QSO host galaxy measured to 30% by *Lacy et al. (2002*) with the existing 3m AO system. This should be a worst-case estimate of the QSO contamination and does not account for the sensitivity gains from the new science detector. Using psf-convolved models of disk galaxies at z<0.5, we estimate a detection limit for these extended sources by scaling the point source sensitivity to account for the larger area, and therefore larger background uncertainty, in these resolved galaxies. We find that a search for DLA galaxies using the new 3m AO system should be able to detect and measure the structural properties of galaxies like those found by *Chun et al. (2006*) out to z=0.3.

1.2 Instrument Overview

1.2.1 Science Camera

The infrared science camera, IRCAL, has imaging, spectroscopic, and polarimetric modes built around a Hawaii RG architecture detector. The detector is a Hawaii-2RG engineering grade device from Teledyne Labs with enough working area to capture the instrument's field of view in both imaging and spectroscopy mode.

The optical design of IRCAL camera remains roughly the same as the original one that fed a PICNIC array. The dewar remains the same as the original, but the detector and optics are changed. The aperture wheel mechanism will be improved to allow better positioning control of the aperture.

IRCAL accepts a non-telecentric f/28.5 beam from the AO system. The camera relay optics consists of an off-axis parabola pair creating an intermediate collimated space that contains a pupil image plane. Two filter wheels are located in the collimated space and a fixed cold stop is located at the pupil plane. An aperture wheel is located at the input focal plane, ahead of the first off-axis parabola but still inside the dewar. The filter wheels in collimated space hold various spectral band and blocking filters, as well as a grism for spectroscopic mode and a Wollaston prism for polarimetric observations. The aperture wheel in the focal plane contains a choice of spectrograph slits for spectroscope mode, a cold finger for blocking a bright source in high contrast imaging, a 100 μm pinhole aperture, and an open position for regular imaging.

1.2.2 Adaptive Optics System

Adaptive optics correction is obtained with a pair of deformable mirrors. The first mirror, the "woofer," provides tip-tilt and low-order (~40 Zernikes) correction at high stoke. The second mirror, the "tweeter," provides the high-order (~700 degrees of freedom) correction but at low stoke. The cascade of stroke and order matches well with the dynamic range presented by the atmospheric turbulence.

Recent advances in silicon micromachining technology have led to the development of a microelectro-mechanical systems (MEMS) deformable mirror that enables high order wavefront correction at reasonable cost. Shane AO uses a 1024-actuator MEMS device (about 750 active actuators in the illuminated pupil) to correct the atmospheric phase aberrations ahead of the science imager. The large number of actuators, more than ten times that of the prior system, provides excellent wavefront correction and leads to very high Strehl across the near- infrared bands with some decent performance in the visible I-band as well.

The wavefront sensor is a Hartmann sensor built around a 160x160 pixel CCID66 high speed, low-noise CCD developed at Lincoln Laboratories. The Hartmann sensor can sample at either 8, 16 or 29 subapertures across the pupil diameter (43 cm, 20 cm and 10 cm subapertures mapped at the primary mirror, respectively). The selection allows for adjusting to laser guide star brightness (sodium density varies seasonally), or to the use of natural guide stars.

The AO system operates in closed loop mode. In closed loop, the wavefront sensor detects the guide star light after it has reflected off of both deformable mirrors. A dichroic splitter divides the light between the Hartmann wavefront sensor and the science camera, with longer wavelengths going to the science camera.

The AO system will be able to operate with both a laser guide star and natural guide star references. In laser guide star mode, a natural star in the surrounding 120 arcsecond diameter field is needed as an absolute tip/tilt reference since the laser beacon does not sense this mode. A beamsplitter in the wide-field relay transmits the natural star light to a separate high-speed tip/tilt sensor, while the 589 nm laser guidestar light goes to the Hartmann wavefront sensor whose pick-off is located in the narrow-field second relay.

1.2.3 Laser Guide Star

The laser provides a guidestar in science target fields where no suitably bright natural guidestar is available. The use of a laser guidestar greatly increases the fraction of the sky over which adaptive optics is useful, from less than 0.1% to over 30%. The dye laser for the Lick 3-meter AO system was the first to be used in astronomy for regular science observations (*Max et. al, Science, 1996*). The ShaneAO system uses a solid-state fiber laser, built by Lawrence Livermore National Laboratory. This laser is smaller, simpler to operate, and produces a brighter guide star than the earlier dye laser system.

The laser beam is launched from a refractive telescope mounted on the side of the Shane 3-meter telescope. It exits the telescope with a beam diameter of 20 cm and produces a guide star at the sodium mesosphere at 90 km altitude with a beam waist of approximately 3 m, or, resolved at the ground, about 1 arcsecond in extent. This is sufficiently "point-like" for the Hartmann sensor to operate as if the beacon were a point source.

The laser beam and resulting guide star are monochromatic at a narrow 589 nm line. Given the dichroic beam splitter arrangements, none of this light should appear on the science detector.

1.3 Observer's Manual

This chapter describes how an observer uses the ShaneAO system to collect astronomical data. Observation generally consists of three steps: 1) observation planning, 2) data collection, and 3) data reduction and analysis. Each of these steps is explained below.

1.3.1 Observation Planning

The observer should carefully plan the observations for the night. Some advance planning and coordination with observatory enable a smooth and somewhat automatic observation sequence. Preparations include:

- Provide a science target list. Using the proper entry format will enable this list to be compatible for interface to the telescope control system, and, in LGS operational mode, for interface to Laser Clearing House for satellite avoidance.

- The observatory provides links to star charts and lists, ephemerides, twilight schedules, zenith and hour angles to help plan observation times.

- The observatory has links to databases to aid in choosing calibrators: e.g. photometric calibrators, astrometric calibrators.

- Sky or dome flats should be scheduled for the evenings/mornings surrounding observation and may include observation during certain allowed hours of twilight. The observatory staff or web site guides aid in planning the correct times and exposures for these.

- The observer will choose candidate tip/tilt stars for use in LGS mode. These will need to be within the tip/tilt radial field accepted by the tip/tilt sensor around the science target.

- A rough exposure time calculator, using the known throughput and emissivity characteristics of the instrument, will be available on-line.

1.3.2 Data Collection

This section will eventually discuss:

- Camera operation
- Means for quicklook of data during observation
- Temporary data location.

1.3.3 Data Reduction

The observatory maintains a long-life database of science data, which is accessible to the observers after observations were recorded. The data is stored in FITS format. Details of the FITS headers will be published as an appendix to this document. Fits header information includes position and status of the telescope, parameters of the science camera exposure, and condition and state of the adaptive optics system.

Archival data location and retrieval process...

The observatory will provide some recommended basic calibration reductions for the IRCAL camera and AO system. Observers are encouraged to contribute tools to the community of ShaneAO observers, which will be made available via web site.

1.4 Instrument Specifications

This chapter summarizes the operating modes, functional capabilities, and key parametric values of the ShaneAO instrument, giving the requirements for the design of the system.

1.4.1 Overall

- The system provides diffraction-limited imaging and spectroscopy in the near infrared wavelength range from 1.0 to 2.2 μm, corresponding to the astronomy science atmospheric transmission bands denoted as J, H, and K.

- The optical path input to the system accepts the f/17 cassegrain feed of the Shane telescope.

1.4.2 Science Camera

- The science camera optics provide diffraction-limited imaging and spectroscopy in the near infrared wavelength range from 1.0 to 2.2 μm, corresponding to the astronomy science atmospheric transmission bands denoted as J, H, and K, and the science detector provides Nyquist sampling of the diffraction limit in J-band.

- The science camera provides an unvignetted square field of view of 20" on a side (corresponding to a circular field of view of approximately 28").

- The science camera will provide grism spectroscopy with a resolution of approximately R=500. Higher resolution is possible with an upgraded grism.

- The AO relay and dewar will have the capability of field rotation (by rotating the telescope tub) in order to orient science objects on the spectrograph slit.

- The science camera will provide the capability to do linear polarimetry with a waveplate external to the dewar and a Wollaston prism located within the dewar.

- The science camera and associated optics will fit in the existing IRCAL dewar.

1.4.3 AO System

Architecture

The Shane 3-m upgrade will adopt the "cascaded-relay" architecture. A wide-field, low-order and tip-tilt corrected relay will pass a 120" patrol-field to the tip/tilt and focus sensors. The central 20" of the field of view will pass through a second, narrow-field, high-order AO-corrected relay. The laser guide star wavefront sensor pick-off will be located in the second relay. IRCAL will be located at the focal plane of the second relay.

Optical

- The AO system accepts the f/17 beam from the Shane cassegrain feed and produces an f/28.5 beam as output to the science camera, allowing for the f/28.5 focus to be inside the IRCAL dewar at the aperture wheel.

- The AO system has a 1024 degree-of-freedom "tweeter" deformable mirror at a pupil conjugate and a low-order "woofer" deformable mirror mirror at a pupil conjugate (i.e. the AO optical relay has two pupil conjugate planes).

- The combination of woofer and tweeter deformable mirrors correct for tip/tilt; there is no separate tip/tilt mirror.

- The beam size at the pupil location of the deformable mirror is 31 deformable mirror actuator spacings. At 340 micron DM actuator pitch, this is 10.54 mm diameter.

- The dichroic split between science camera path and wavefront sensor path is after the deformable mirror.
- The "centerline" of the AO optical system is defined as that corresponding to the centerline of the Shane telescope cassegrain feed and is the same as the centerline of the IRCAL science camera.
- The tip/tilt sensor light path is split after the woofer deformable mirror.
- The tip/tilt sensor path is steerable for field selection of the tip/tilt star over a 60 arcsecond radius around the optical system centerline.
- The wavefront sensor light path is split after the tweeter deformable mirror.
- The wavefront sensor path is steerable for field selection of a guide star over a 14 arcsecond radius around the optical system centerline.
- Wavefront sensor field selection steering and tip/tilt sensor field selection steering are independent of each other.

Calibration

- When the system is dismounted from the telescope and in the laboratory, the system will have an atmosphere and telescope simulator that provides a beam identical to the Shane 3-meter telescope f/17 beam, simulated natural and laser guide stars, and moving atmospheric phase plates at ground and 5 km conjugates. This will be used during laboratory alignment of the system, not while on the telescope.
- The system will have the ability to move into place a calibration source at the telescope focus. The source will move completely out of the way to clear the entire AO system field of regard (60 arcseconds radius) during on-sky observation.
- The calibration sources are:
  - laser (any line between 630-660)
  - white light broadband covering 500 to 2200 nm.

Electronic

Wavefront Control System

- The AO reconstructor accepts input from the wavefront sensor camera and the tip/tilt sensor camera and produces outputs for both the woofer and tweeter deformable mirrors.
- The AO controller operates at up to 2kHz frame rate.
- The AO control loop has the following latencies: 500 microsecond camera exposure, 500 microsecond camera frame read, 500 microseconds compute latency and data transfer to DM driver.
- The AO control loop can operate at frame rates from a maximum of 2kHz to a minimum of 50 Hz.
- Details of the real-time control algorithm:
  - **Camera data processing: background subtraction and flat-fielding** correction.
  - Centroiding of Hartmann spots on a 4x4 pixel grid
  - **Slope-to-phase computation using an approach that allows for modal** weighting, minimum variance estimation, and waffle-mode suppression.
  - **Wind prediction and forward wavefront control adjustment for the** wind (See *Johnson, 2010*).
  - **Proportional-Integral feedback control, in the phase (actuator)** space.
  - Lead-lag compensation.

- – Adjustable lead-lag weights.

- – **Plate-equation and non-linearity compensation for the MEMS** deformable mirror.

- – **Separation of low order wavefront control from higher order** wavefront control and transfer of these signals to the woofer and tweeter DM accordingly.

- – **In laser guide star mode the ability to sense tip/tilt using the** natural guide star tip/tilt sensor.

- – **In laser guide star mode the ability to sense the tip/tilt portion** of the LGS Hartmann sensor signal and use it to drive laser beam "uplink" tip/tilt.

Optical Bench Automation

The AO optical bench automation is as follows:

- Input beam steering from the telescope allows adjustment of the incoming beam for co-registration of telescope pupil to AO system pupil to an accuracy of 0.01 of a pupil diameter and a range of 1 pupil diameter. (Given that telescope pointing co-registers the focal center points.)

- Calibration insertion blocks the telescope beam and provides light from calibrator sources.

- The moving phase plates in the atmosphere and telescope simulator can run at a simulated 90 m/sec maximum speed down to 0 m/sec minimum speed with adjustment to a resolution of 1 m/sec.

- Field steering, pointing and centering, for the natural tip/tilt star. This is steerable to up to 60 arcseconds off-axis of centerline to an accuracy/resolution of 0.1 arcsecond in pointing and 0.01 aperture diameter in centering.

- Field steering, pointing and centering, for the wavefront sensor guide star. This is steerable up to 10 arcseconds off-axis of centerline to an accuracy/resolution of 0.1 arcsecond in pointing and 0.01 aperture diameter in centering.

- Science path pointing and centering. This is steerable up to 10 arcseconds off-axis of centerline to an accuracy/resolution of 0.1 arcsecond in pointing and 0.01 aperture diameter in centering.

- Science path focus is not adjustable but is aligned to a focus accuracy corresponding to less than 250 rms (1/4 wave at 1 micron wavelength) wavefront error. This is computed to be <250 microns in the f/28.5 beam.

- Hartmann sensor focus. Adjustable from 80 km focus to infinity focus with resolution of 1 km. This is continually on and adjusting during an exposure in laser guidestar mode.

- Polarimetry wave plate. Rotation stage adjustable over 360 degrees with an accuracy of 0.1 degree.

Deformable Mirrors

The cascaded relay design facilitates woofer/tweeter AO correction by providing two optical planes conjugate to the telescope pupil. Both pupil planes are located in collimated (with respect to the science light) spaces.

The woofer, an ALPAO Lo-speed DM 52, will have adequate stroke and bandwidth to provide both tip/tilt and low-order wavefront correction. The ALPAO Lo-speed DM52 has 52 actuators on a 2.5 mm pitch, for a maximum pupil diameter of 15 mm. It has 45 microns of surface tip/tilt peak-to-valley stroke at >200 Hz.

The tweeter DM, a Boston Mircromachines MEMs mirror, lies in the narrow-field second relay. It has 32x32 actuators on a 340 micron pitch, providing a 10.88 mm maximum pupil diameter. The MEMs device has 3 microns of mechanical multi-actuator stroke with bandwidths > 1 kHz.

Tip/tilt Sensor

The pick-off for the tip/tilt/focus (TTFS) sensors will be located upstream of the focal plane of the 120" wide-field relay. The entire 120" diameter will be utilized as a patrol field for tip/tilt stars.

The tip-tilt pick-off will consist of a dichroic beamsplitter that reflects science and laser guide star light and transmits tip-tilt light to the tip-tilt sensor.

Beyond the pick-off, the TTFS relay will contain a reformatting lens to achieve the desired plate scale on the TTFS camera. This lens could be astigmatic if it is determined that focus sensing should be done by introducing astigmatism into the TT sensor beam. A small part of the light may also be picked here and directed to a separate truth wavefront sensor.

The detector of the TT sensor will remain the Scimeasure Little Joe that is currently part of the Lick 3-meter AO system. The current plate scale on the 80x80 detector of 0.33"/ pixel will also be adopted.

Laser/natural Guide Star Wavefront Sensor

After the collimating optic of the second relay and the tweeter deformable mirror, will be a selection of dichroics directing light to the laser/natural guide star wavefront sensor (WFS).

The WFS relay will contain a focusing lens to provide the WFS field stop with a focus. Between the focusing lens and the WFS field stop are a point-and-center pair of field steering mirrors. The WFS package must translate along the optical axis to accommodate focus shifts due to laser guide star zenith distance or operation in natural guide star mode.

The wavefront will be sampled at three scales depending on light levels of the reference source: 8x8, 15x15 and 29x29. The wavefront sensor camera will be a 160x160 pixel Scimeasure CCID66 with 21 μm pixels. Each subaperture will contain 4x4 pixels with a one pixel guard band.

Dichroic Selection for Science Operations

Dichroic passbands and specifications are officially stated in two spreadsheets "dichroics_worksheet.xls" (*KT* *link*) and "3mAO_dichroic_specs" (*KT* *link*). The first dichroic is used to select light for the tip/tilt sensor and the second shares the light between science detector and wavefront sensor.

The tip/tilt sensor is designed to use 600-900 nm wavelength light so the tip/tilt dichroic splitter is a 600-900 nm band pass in transmission. In NGS mode, a mirror is in place of this dichroic.

The wavefront sensor is designed to use 589 nm light in laser guidestar mode and 600-900 nm light in natural guidestar mode. The wavefront sensor dichroic is selected accordingly: a 589 narrow band reflection for LGS and 600-900 nm reflection for NGS.

The infrared science bands z, y, J, H, and K are served by the nominal dichroic selections in either LGS or NGS mode.

The astronomical I band goes down to 700 nm, so a different dichroic science/wfs dirchroic will need to be used for NGS observing. For cost and complexity reasons we are making provision for only two positions in the science/wfs dichroic selector, so for the special situation of I band science observations using a natural guide star, the existing NGS dichroic can be replaced manually.

LGS observing will be possible in I band if the TT dichroic is also replaced with a custom beamsplitter. However, this limits the tip/tilt sensitivity since I band light needs to be shared with the science arm. Purchase of the two additional dichroics needed for I band NGS and LGS science is a future upgrade option.

Table 1. Dichroic selection

Observing Mode	Science	Dichroic 1 (T to t/t sensor)	Dichroic 2 (R to WFS)
LGS	yzJHK	T 600-900	R 589
NGS	yzJHK	Mirror	R < 900
LGS	I	T 600-700	R 589
NGS	I	Mirror	R < 700

1.4.4 Laser and Projection System

- Power: The laser output power is at least 9 watts at sodium D2

- Spectrum: consists of 9 narrow band CW lines separated by >200 MHz. "Narrow band" is less than 1 MHz. The line energies peak in the center and taper on a triangle shape on either size of center. Labeling the lines -4,-3,-2,-1,0,1,2,3,4, the lines have strength: 4, 8, 12, 16, 20, 16, 12, 8, 4 percent of the total laser power, respectively.

- Pulse formats: 1) pulsed at 2.7 kHz with a pulse width of 30 microseconds during which it is CW. 2) pulsed at 10 kHz with a pulse width of 3 microseconds during which it is CW. (Note: mode 2 is the present nominal design)

- Polarization: The laser output is linear polarization. Degree of linear polarization (Stokes $Q2+U2I$) > 99%. The laser projection system converts to circular; see below.

- The laser is remotely adjustable in wavelength for up to 5 GHz either side of the sodium D2 line with no reduction in output power.

- The laser has automatic wavelength control to keep centered at the sodium D2 line to an accuracy of 50 MHz.

- The sodium beacon generating laser is located on a stable platform off of the telescope.

- The high-power 589 nm laser light is fed from the output of the laser to the launch telescope via single mode polarization preserving optical fiber.

- The beam launch system enlarges the beam to 20 cm diameter for projection.

- The beam launch system has diagnostics for pointing and centering of the beam through the launch telescope with a range of 120 arcsec diameter for pointing, 1 beam diameter for centering, and an accuracy/resolution of 1 arcsec for pointing and 0.1 beam diameter for centering.

- The beam launch system has remotely operated beam pointing and centering mirrors. The mirrors are adjustable with a range of 120 arcsec diameter for pointing, 1 beam diameter for centering, and an accuracy/resolution of 1 arcsec for pointing and 0.1 beam diameter for centering.

- The beam launch system converts the output beam to circular polarization.

- For experimental purposes, the beam launch system has a mode that projects linear polarization. The switch from linear to circular polarization is remotely controlled.

1.5 Operator's Manual

This section is to be completed prior to delivery of the instrument.

1.5.1 Instrument Mounting and Power Up

There are two types of power up: one when you mount AO system on telescope, the other on a nightly basis. We will utilize programmable power strips which are controlled remotely via the internet for all the below-mentioned devices.

1. Power up computers: All computers should be able to boot independently, so specific order does not matter. Start up all serving software, including motor control servers.

2. Power up motors, motor controllers, start up motor server (order depends on motor controllers selected).

3. Boot up the real-time computer (RTC).

4. Power up the cameras: wavefront sensor (WFS), tip/tilt/focus sensor (TTFS), and science camera (IRCAL). Note: need to check that the science detector and camera dewar is cold before turning on, so temperature sensor needs to be powered up before science camera.

5. Power up the deformable mirrors (DMs): woofer and tweeter.

6. Power up calibration sources.

7. LGS: Laser system has its own power-controls. The laser system uses an integrated Labview-based controller that does all status monitoring. A qualified laser technician must be present to supervise the laser startup. The Labview service software wrapper will broadcast its state using the Keyword system standard at the observatory. These broadcasts will be accessible by the AO system top-level controller so that laser status is coordinated with AO status, and with FITS header information.

8. There is an independent laser interlock safety system. Independent means, for safety, the system operates regardless of the state of any other computer or the network (although it does report status over the network, this status is not relied on for safety).

Software Startup Procedure

Science Camera

(a) i. Setup user interface allows selection of IRCAL exposure time, filter wheel, aperture wheel, mosaicing or dithering pattern. During engineering, selection of region of interest and rapid readout modes are required. For science, slow readout with low noise is preferred.

2. Need to define combinations of dichroics/filters/states that conflict so software can alert user (for example, using same wavelength band for tip/tilt and science).

3. UI also allows co-adds of images, "snappy-diffs" (quick difference images with a micro-dither in between them for image location).

4. Quicklook on existing system allows check for overexposure, background. This could also indicated intensity at which detector becomes non-linear (less than saturation point). This is a cursor-based system presently. We may want to color-code saturated or non-linear pixels.

5. Logs – logging every exposure is a FITS file with a header. Need to determine header information, where data is stored, when data is stored, when header is written. A table with explanation of each header value is useful. Also should include observer's autolog, single line for every exposure with your choice of information. Object name and comment field must be filled in by observer. Comments may not occur in FITS header, but should be in autolog.

6. Need to provide observers with location of data, location of autologs. Also may include environmental data not in FITS headers.

AO System

1. Servers, software and GUIs should start up automatically, even if on different computers. We should not have to start each program individually. Software includes RTC, GUIs, telemetry pipeline.

2. Check clocks to make sure all system clocks agree.

Calibrating the AO System

1. Make sure you have flat for WFS. If not, with calibration source not in path, record a background signal for the WFS.

2. Make sure you have current control matrix for WFS.

3. Turn on and move in calibration light source (CLS) at telescope focus.

4. Center CLS on IRCAL camera by moving CLS (need to make sure in software that IRCAL filters are out and exposure time is appropriate).

5. Adjust WFS pointing and centering until CLS well-aligned on WFS. WFS tip-tilt readings should be small. Subapertures should be evenly illuminated.

6. Close TT loop on WFS TT signal.

7. Take exposure on IRCAL science camera and measure position of CLS.

8. Adjust pointing and centering into WFS until CLS hits same spot on IRCAL as it did in step 6.

9. Put in white light source, and adjust position until tip is 0.

10. Optimize exposure time on WFS until desired intensity reached (existing system this was 1500 counts per subap).

11. Close TT and AO loops.

12. Perform image sharpening to Strehl > 0.9 on white light source.

Acquiring a Guide Star / Science Target

1. Guider is co-referenced to IRCAL science detector frame so it will reliably set science position.

2. After a long slew, pointing errors are possible. Use the following pointing correction:

    (a) Slew to a V < 8 star near the science target (within 1 degree).

    (b) Match telescope pointing location of the star with catalogued coordinates.

    (c) Repoint the telescope to science target with newly calibrated pointing.

3. Find tip/tilt star in guide camera.

4. Move telescope to science field of view

5. Verify science target location with "snappy diff".

6. Move field steering mirrors of TTF sensor, based on known position of science object with respect to tip/tilt star, to center TTS on tip/tilt sensor.

7. Adjust telescope focus to focus TT star on TT sensor.

8. If in NGS mode, move WFS field steering mirrors, based on known position of science object with respect to NGS, to center NGS on WFS field stop. In most cases in NGS mode, the science object will be the NGS.

9. Offset the telescope to blank sky to record a TT/WFS background signal.

10. Go back to telescope pointing which places science object at center of IRCAL.

11. Close the TT/woofer loop (woofer handles TT and low-order). If LGS, TT signal comes from TT sensor. If NGS, TT signal comes from NGS WFS.

12. Close the MEMs loop.

Projecting the Laser

1. Verify that conditions are acceptable for laser projection (radio communication with airplane safety spotters, lasing is good-to-go regarding satellite avoidance.)

2. Propagate laser.

3. Adjust focus stage of wavefront sensor (WFS) based on zenith distance of target.

4. Check laser guide star return signal levels on the wavefront sensor. If there is an error in relative positioning between the laser launch mechanisms and the wavefront sensor boresite, the signal may be low. If signal is low, repoint laser launch in a search pattern.

5. Tune off sodium line and acquire a background Rayleigh backscatter signal for the wavefront sensor.

6. Close the woofer control loop, tip/tilt mode, on the tip/tilt star (acquired in step 6).

7. Close higher order wavefront control loop (woofer and tweeter DMs).

Optimizing the Control Loops

1. Optimize WFS frame rate, given signal level and seeing.

2. Optimize loop gain (goal is to have this automated using real-time-controller's (RTC) telemetry data analysis).

1.6 Laser Technical Manual

This section is to be written prior to delivery of the laser.

Operator's Qualifications and Safety Considerations

System Startup

System Calibration

1. Pulse timing

- Wavelength

    Observing Operations

1. Tuning off and on sodium wavelength

1.7 Design Document

1.7.1 AO Optical

First Order Optical Layout

The adaptive optics system will be mounted at the Cassegrain focus of the Shane 120 inch telescope. Best-known parameters of the telescope Cassegrain focus are given in Table 2.

Table 2. Shane 120" telescope Cassegrain focus parameters.

Mirrors	Primary, secondary
	Coating: Aluminum
Primary	Radius of curvature: 30.5 m
	Diameter: 3.048 m
	Conic constant: -1
Secondary	Primary-secondary distance: 11.47 m
	Final focal length: 53.410 m
	Radius of curvature: 10.58
	Conic constant: -3.238 (estimated)
	Focal radius of curvature: 4.135 m
	Diameter: 0.9 m
Output beam	Focal ratio: 17.52
	Exit pupil location:16.866 before focus
	Exit pupil size: 0.963 m
Plate Scale	0.259 mm/"
Focus Location	1.778 m behind primary

An annotated layout of the ShaneAO optical relay is shown in Figure 1. Each component of the optical system will be discussed in detail in the following sections.
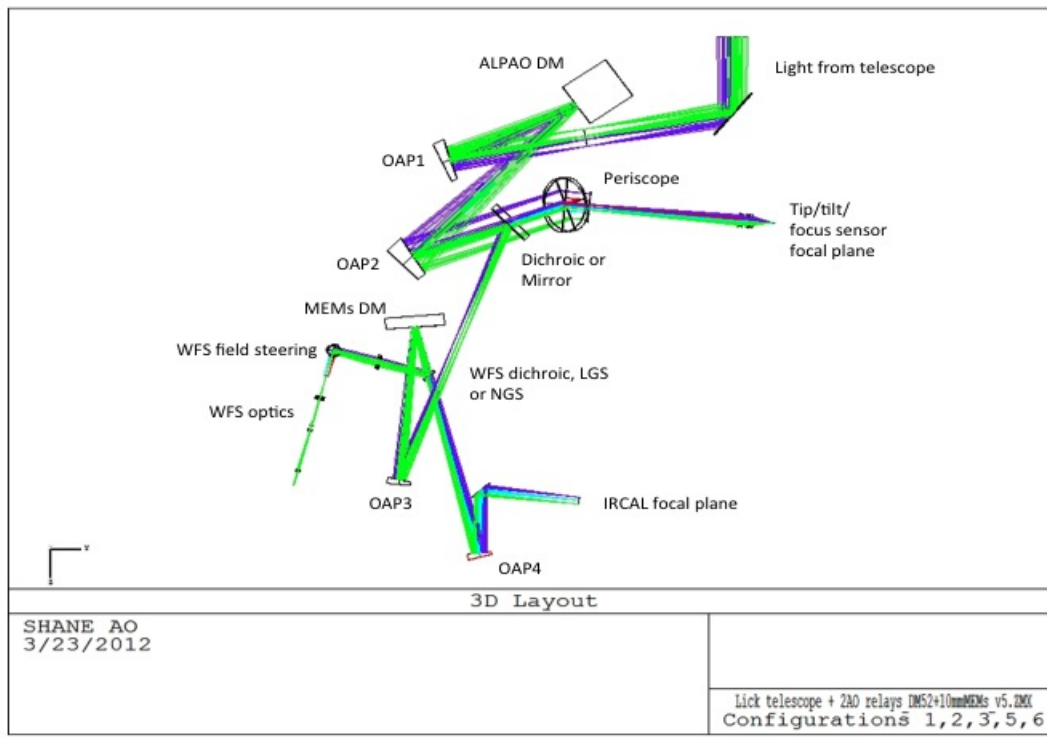
Figure 1. Annotated optical layout of the AO relay.

Light from the telescope enters from the top of Figure 1 with a focal ratio of f/17-f/18, depending on secondary mirror position. The system has been designed for f/17.5, corresponding to the midpoint of the secondary travel.

The first, unmatched-OAP relay contains a 15 mm diameter low-order deformable mirror (DM) conjugate to the telescope primary and transmits a field-of-view (FOV) of 120" with an f/28.5 output.

A dichroic beamsplitter transmits light to the tip/tilt/focus sensor (TTFS), located after the focal plane of the first relay, providing a 120" patrol field for the tip/tilt reference star. The reflected light goes on to a second, matched-OAP relay containing a 32x32 actuator MEMs high-order DM, also conjugate to the telescope primary, and transmits an unvignetted 28" diameter FOV to the IRCAL science instrument A dichroic beamsplitter located in collimated space after the high-order DM directs non-science light to a wavefront sensor which can be used with both natural and laser guide stars.

First Relay

The first relay consists of two unmatched off-axis parabolas which, given an input beam of f/17.5, provide an output f/28.5 output focal ratio. The first parabola produces, in collimated space, a plane conjugate to the primary mirror at which the 15 mm low order DM is placed. The second OAP of the unmatched pair relays the Cassegrain focus to a second focal plane, with a focal ration of f/28.5. Near the focal plane of the OAP relay is a fixed 2-mirror periscope, directing the light to the tip/tilt/focus sensor. Preceding the periscope is a pick-off to send light to the second relay. The pick-off consists of a dichroic beamsplitter during laser operation, when the tip/tilt sensor is used, and a mirror during natural guide star observations.

For pupil alignment to the telescope, an additional fold mirror is located in the converging space before Cassegrain focus. During initial mounting to the telescope, the telescope pointing and this first fold mirror act as a pointing and centering pair.

Calibration Source and Acquisition Camera

The first focus of the adaptive optics system will contain a selection of fiber sources to use during calibration and alignment of the system. These include a white light source and a red laser diode source. An acquisition camera is also located at the Cassegrain focus. This camera will be a Point Grey GigE Flea3 with a ½ inch sensor. At the 0.259 mm/" plate scale this camera will image a 49" field-of-view. It is intended for use during initial alignment to the telescope, and as a reference between the adaptive optics system and the 3-meter TUB guide camera.

Off-axis Parabolas

To first order, OAP1 has an apparent focal length that meets the requirement of a 15 mm pupil on the low order DM. The focal length can be found by the following relation,

		1.

where d_{DM} is the low order DM pupil size of 15 mm, d_{PM} is the primary mirror size of 3.048 m, and F_{tel} is the focal length of the telescope, 53.410 m. This gives a focal length for OAP1 of 262.8 mm.

The low-order DM follows OAP1 at a distance from OAP1 that will place it conjugate to the telescope primary, or

	,	2.

where t_{pupil} is the distance to the telescope exit pupil from the telescope focus. Equation (2) gives a total OAP1 to low-order DM distance of 266.9 mm.

Finally, in order to match the current input f/# to IRCAL, we'll need a slight magnification in the AO relay. It's advantageous from a packaging standpoint to use OAP2 to achieve this magnification. To first order, the focal length of OAP2 will be given by

	,	3.

where $f/\#_{out}$=28.5 and $f/\#_{in}$=17.5, giving a focal length for OAP2 of 428 mm.

The numbers derived with Equations (1), (2), and (3) are first order approximations only. In fact, the pupil on the deformable mirror is undersized to account for many variables, including an uncertainty in the input f/# of the telescope, and also for elongation due to the DM's tilt and pupil aberrations. Also, the focal lengths and distances derived above assume the parabola is used on-axis. The parent focal lengths (see Figure 2) of the off-axis parabolas were determined using Zemax. Table 3 gives actual specifications, determined in Zemax, for each of the optics in the AO relay.

Figure 2 Diagram of off-axis parabola (delineated by black cut-out) with respect to parent parabola.

Table 3. OAP specification for Shane AO

	Radius of Curvature (mm)	Diameter (mm)	Off-axis Distance (mm to center)
OAP1	456.0	75	60.0
OAP2	742.0	75	167.3
OAP3	549.6	40	77.2
OAP4	549.6	40	77.2

Woofer Deformable Mirror

Low-order wavefront correction and tip/tilt are achieved with an ALPAO DM52-25-2.5 voice-coil actuated deformable mirror, shown in Figure 3. The mirror has 52 actuators on a 2.5mm pitch, and a useable pupil diameter of 15 mm. Its measured tip/tilt stroke is 40 μ P-V, surface, shown in Figure 4, and its inter-actuator stroke 8 μm P-V.

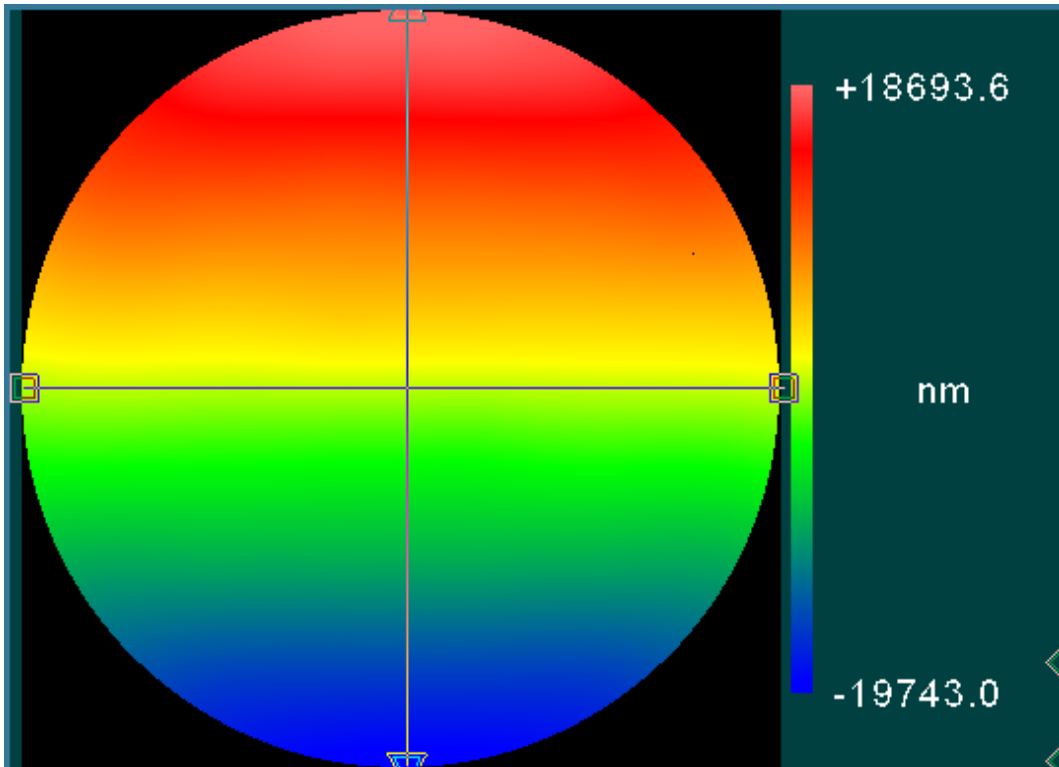Figure 3. Woofer DM: ALPAO 52-actuator magnetically actuated membrane deformable mirror.

Figure 4. Measured tilt stroke, displayed as surface in nanometers.

The mapping of the pupil on the mirror, and the mapping of the subapertures (in 8 x 8 sampling) is shown in Figure 5. Due to the 10° angle of incidence, the pupil is slightly (2.2%) elongated in the direction parallel to the optical table.
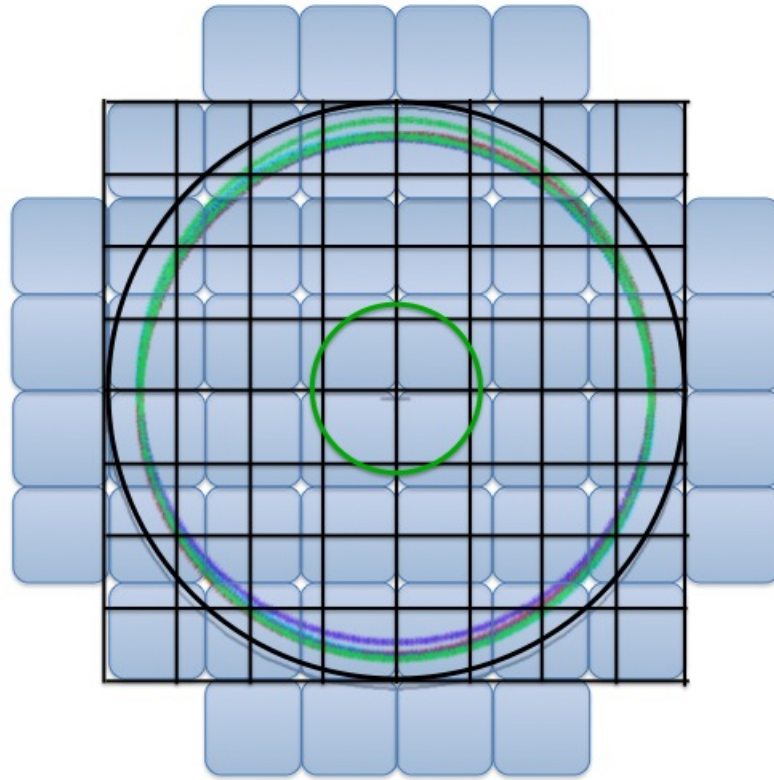
Figure 5. Mapping of the pupil (green/purple annulus) and subapertures (black grid) on the DM52. The actuators are shown as blue pads, with the 15 mm clear aperture of the membrane a black circle.

In Figure 5 the pink annulus represents the pupil imaged on the woofer. The black grid is the wavefront sensor subapertures, and the blue pads represent DM actuators. The ALPAO DM is coated with protected silver, having the reflectance characteristics show in Figure 6.

Figure 6. Measured reflectance of the protected silver coating on the ALPAO DM52-25.

Tip/tilt/focus Sensor (TTFS)

Laser guide stars do not provide an absolute reference object for tip, tilt and focus. During laser operation, a natural guide star is required to obtain the tip, tilt and focus information for correction of image motion and blurring.

Optical Feed

In the converging beam after OAP2 the science and laser guide star light is directed to a second OAP relay by a dichroic beamsplitter. During natural guide star adaptive optics operations, the dichroic beamsplitter is replaced by a mirror because a separate tip/tilt reference is not required. The dichroic beamsplitter allows transmission of visible wavelength light to the tip/tilt/focus sensor, while reflecting the J, H, and K bands to the science detector. The beamsplitter also reflects the laser guide star sodium wavelength (0.589 μm) to the second relay where the wavefront sensor is located.

Figure 7 shows a design-theoretical curve provided by Custom Scientific for a TTFS dichroic beamsplitter with a guaranteed reflectance >99.5% at 589 nm. A dichroic beamsplitter that allows I-band science observations has also been specified for a future upgrade to visible light adaptive optics.
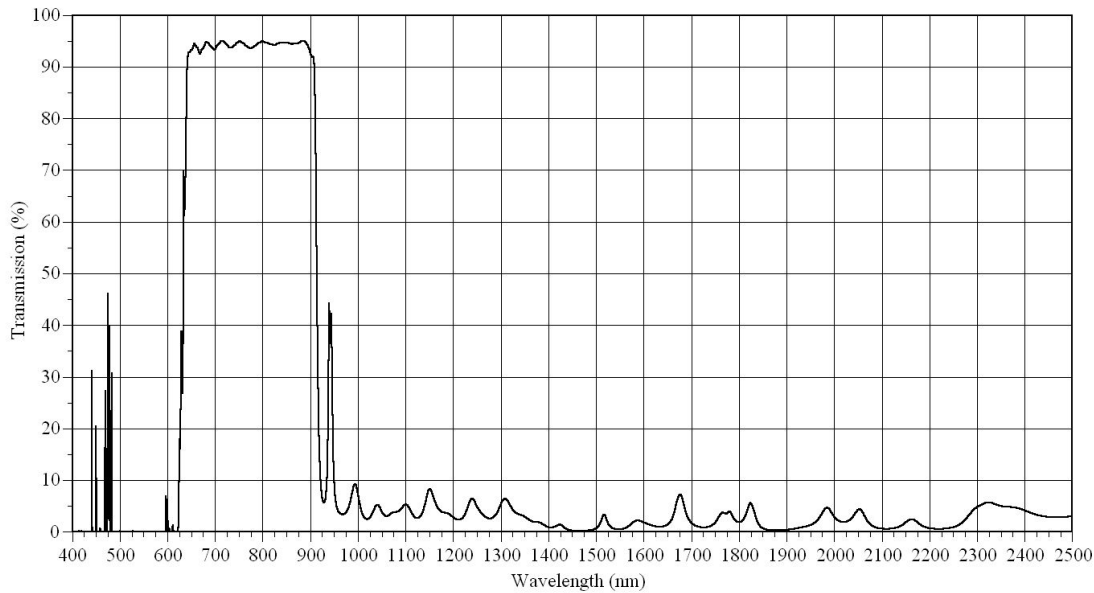
Figure 7. Theoretical transmission curve for the TTFS dichroic beamsplitter.

The converging beam from the first relay is steered by a fixed periscope to send the natural guide star light through to the tip/tilt sensor. The beam is reformatted by an achromatic doublet in order to achieve an acceptable plate scale on the tip/tilt sensor. Currently, and in the upgraded Shane AO system, the tip/tilt detector is the Scimeasure Little Joe, an 80x80 detector with 24 micron pixels. The pixels are binned 3x3, and have a plate scale of 1"/binned pixel, or 0.072 mm/arcsecond. To achieve the 0.072 mm/arcsecond on the tip/tilt detector will require a magnification of 5.84 for an effective f/# of 4.87 into the tip/tilt detector. Both the doublet and the Scimeasure detector are mounted on large-travel x-y stage that is able to patrol the entire field-of-regard.

The Zemax drawing of the tip/tilt/focus sensor path is shown in Figure 8
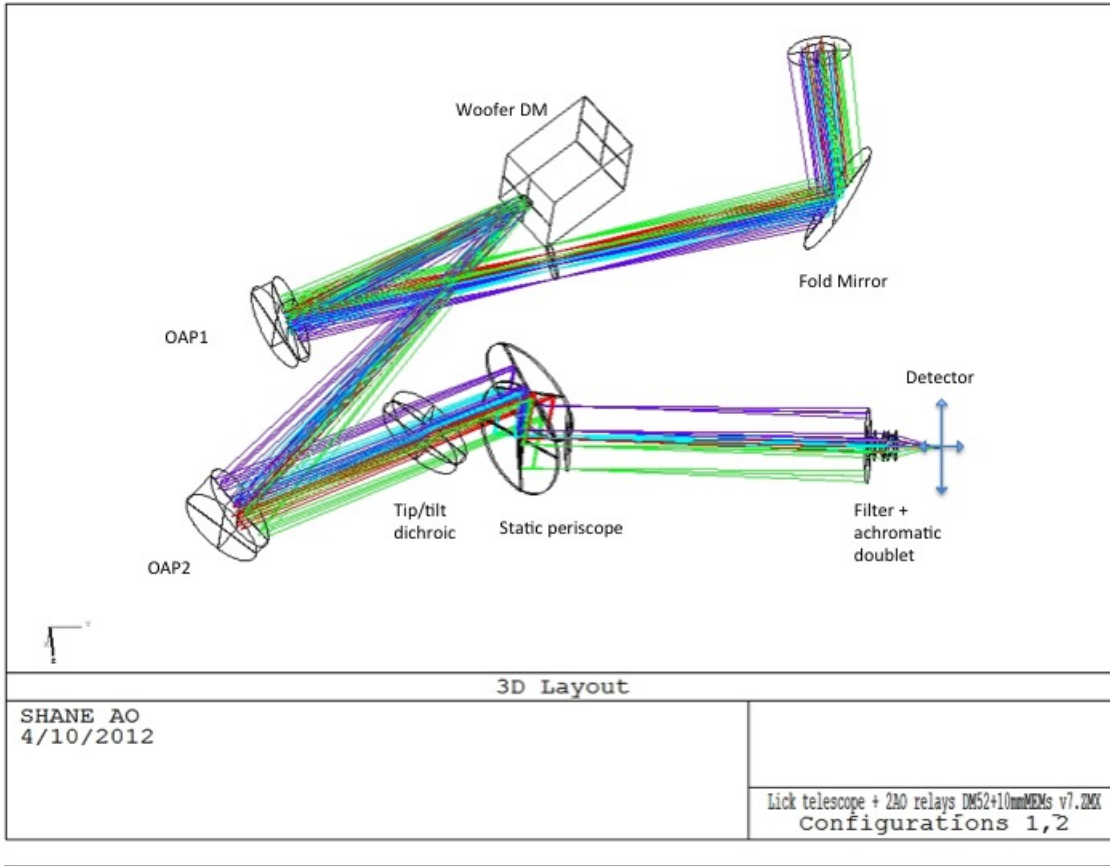
Figure 8. Optical path to tip/tilt/focus sensor. Cassegrain input is at top of figure.

Slow-Focus Sensing Method

There is a requirement in the Shane AO system for slow focus sensing of a natural guide star. This can be accomplished by adding an astigmatic lens to the optical path of the tip/tilt sensor, at an orientation of 45° to the detector pixels. When the beam is in focus, the image on the detector will be exactly in between the saggital and transverse foci, with a diameter equal to the circle of least confusion. As the beam is defocused, the image will appear as an ellipse, then a line focus as it approaches either the saggital or transverse focus. The orientation of the line will be at ±45° to the detector pixels depending on the direction of defocus. The Zemax generated through-focus spot diagram in Figure 9 displays this effect.
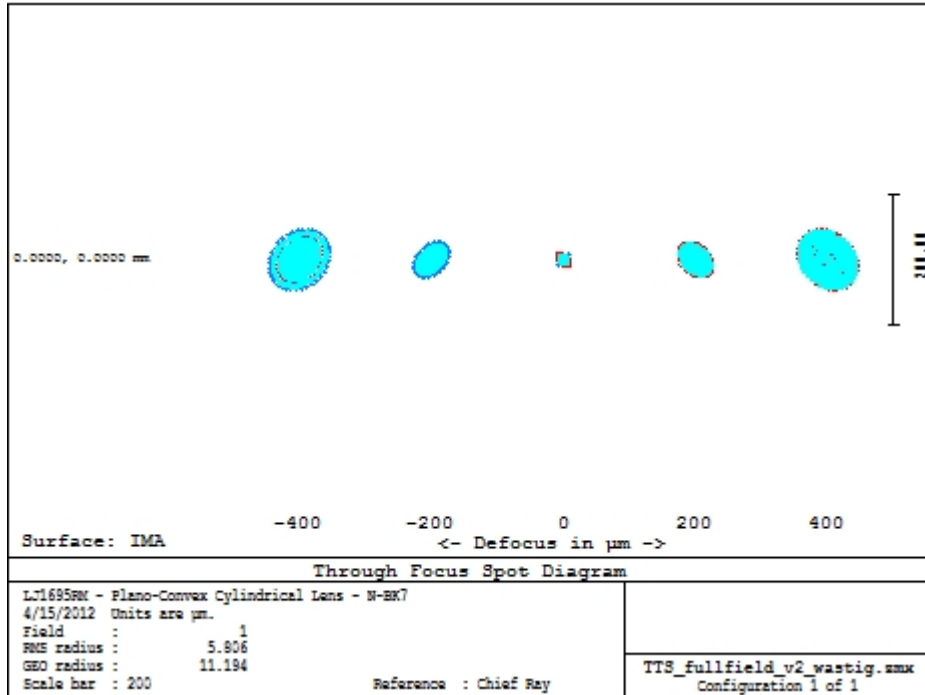
Figure 9. Example of through-focus behavior of spots on tip/tilt/focus detector when a cylindrical lens is added to the optical path near the reimaging lens.

Second Relay

The purpose of the second relay is to relay a 28" diameter science field of view (inscribed square of 20" on a side) to the IRCAL focal plane, and relay an approximately 10 mm pupil image to the high order deformable mirror. The second relay consists of two matched off-axis parabolas which provide an f/28.5 output focal ratio into IRCAL. The first parabola produces, in collimated space, a plane conjugate to the primary mirror at which the 32x32 actuator, high-order DM is placed. A second OAP, matched to the first, produces a final focal plane located at the IRCAL aperture stop (within the IRCAL dewar). In the collimated space after the deformable mirror is a selectable dichroic beamsplitter, reflecting light to the laser/natural guide star wavefront sensor.

Off-axis Parabolas

To first order, OAP3 has an apparent focal length that meets the requirement of an approximately 10 mm pupil on the low order DM. The focal length of OAP3 can be found with , giving a focal length of 285 mm for a pupil diameter of 10 mm on the MEMs. The beam entering the second relay is telecentric, so the pupil image is located one focal length away from OAP3.

The second relay maintains the f/# produced by the first relay as this is the legacy f/# going in to the IRCAL science instrument. OAP4 is therefore matched in focal length and off-axis angle to OAP3 (see Table 3).

Tweeter Deformable Mirror

The high-order tweeter DM is a Boston Micromachines 32x32 actuator Kilo-DM. The actuators have a 0.340 mm pitch for a clear aperture of 10.88 mm. A photo of the Kilo-DM is shown in

. The bandwidth of the DM is several kilohertz, with a measured single-actuator stroke of 900 nm and a grouped actuator stroke of nearly 2 microns (Figure 11).
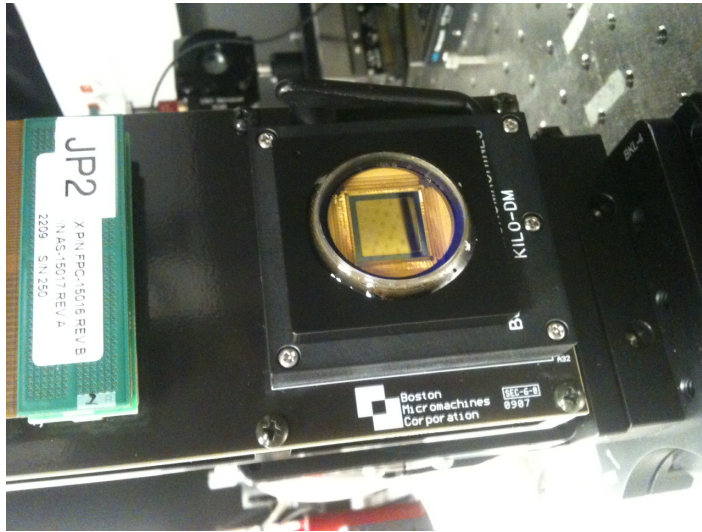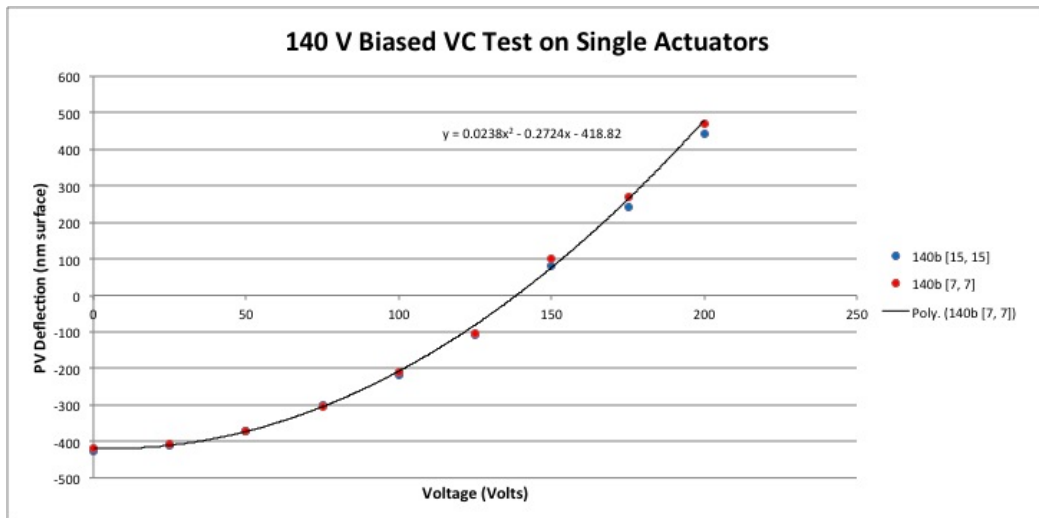

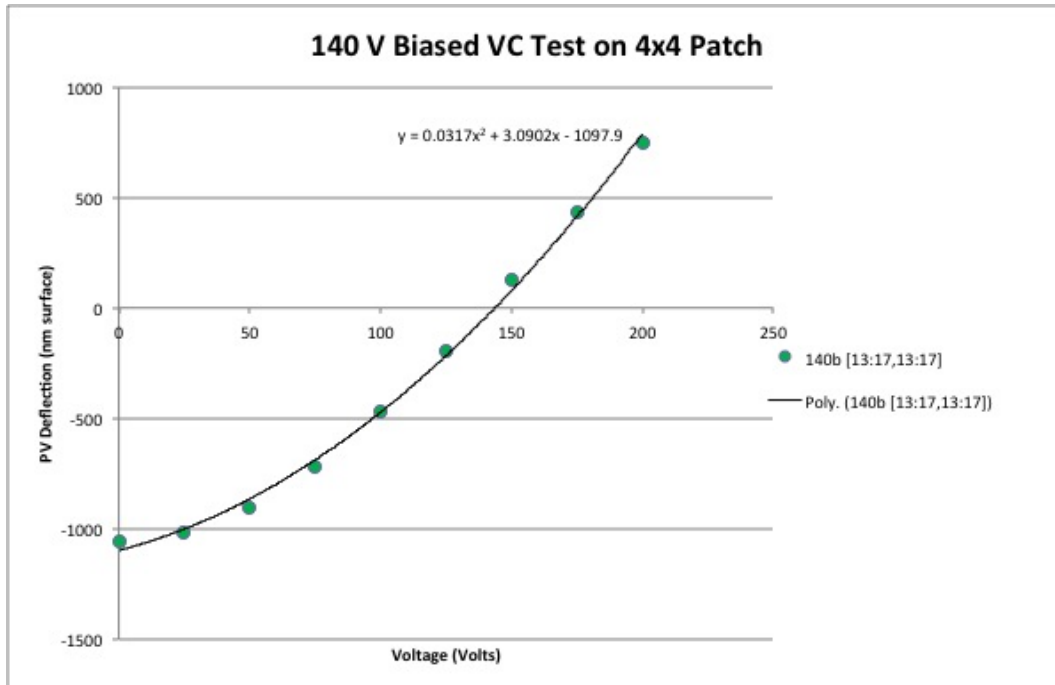Figure 10. The Boston micromachines Kilo-DM under test at the Laboratory for Adaptive Optics.

Figure 11. Measured stroke of the Kilo-DM both for a single actuator (top) and a 4x4 group of actuators (bottom).

The continuous mirror facesheet is gold-coated, giving optimum reflectance for the near-infrared science light.. For environmental reasons (the MEMs DMs require low-humidity), a window is mounted to the front of the deformable mirror. The window is tilted 5° to divert ghost reflections to baffles, and AR coated to maximize transmission in both the IR and at 589 nm (since the wavefront sensor is located after the DM). The measured reflectance curve for the MEMs mirror is shown in Figure 12

Figure 12. Measured reflectance for the MEMs window anti-reflection coating. Y-axis is percent reflection, x in wavelength in nanometers. .

The mapping of the pupil on the MEMs device, and the wavefront sensor subapertures in 8x8, 16x16, and 32x32 subaperture mode are shown below in Figure 13, Figure 14, and Figure 15. Due to the 10° angle of incidence on the deformable mirror, the pupil will be elongated by approximately 2% in the direction parallel to the optical bench. This slight elongation is included in the figures.
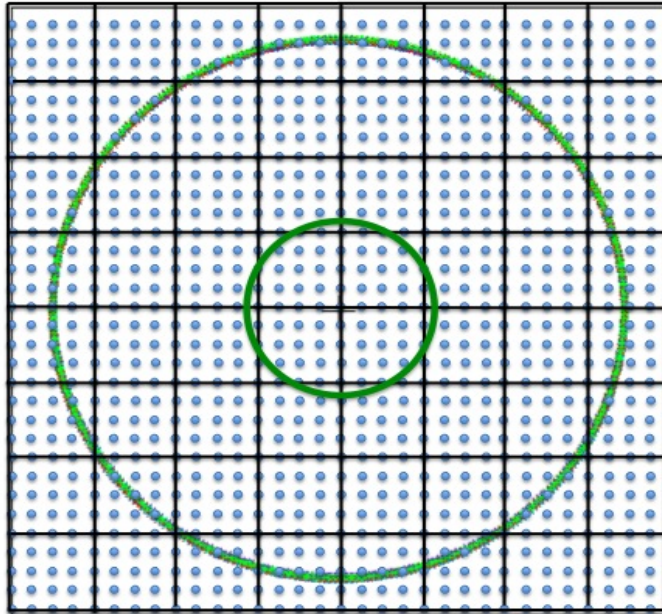
Figure 13. Pupil mapping (green annulus) on the 32x32 MEMs device (actuators are blue dots) for the 8x8 subaperture case (black boxes are subapertures).
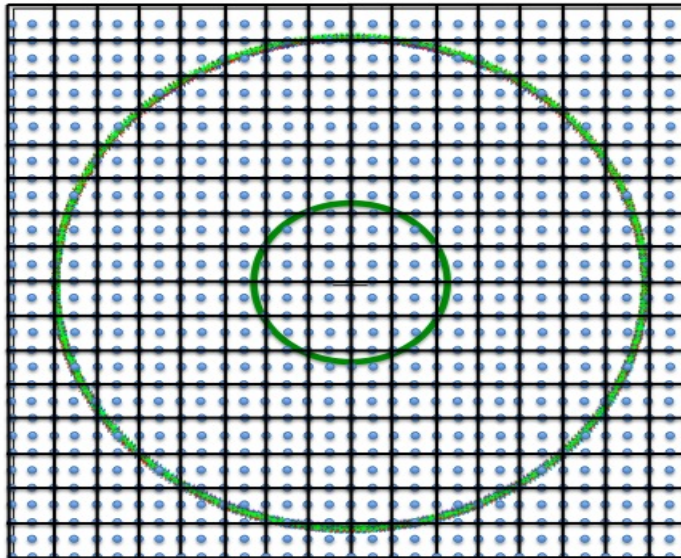

Figure 14. Pupil mapping (green annulus) on the 32x32 MEMs device (actuators are blue dots) for the 16x16 subaperture case (black boxes are subapertures).
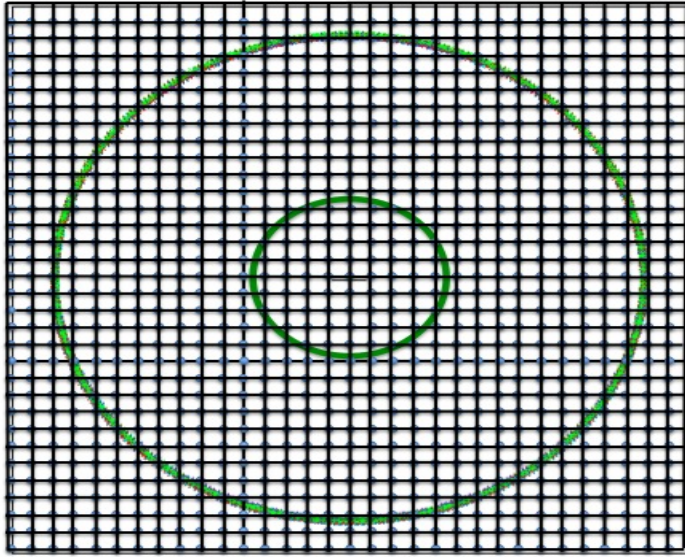
Figure 15. Pupil mapping (green annulus) on the 32x32 MEMs device (actuators are blue dots, and are located at the corners of the subapertures) for the 32x32 subaperture case (black boxes).

Wavefront Sensor Pick-off

Following the MEMs deformable mirror is the pick-off to the laser/natural guide star wavefront sensor. With the wavefront sensor pick-off located after both deformable mirrors, the system will be able to operate in closed loop control.

The pick-off will contain a choice of dichroic beamsplitters, depending on whether the observations use a natural or laser guide star, and the desired band for science observations. Theoretical transmission/reflectance curves for beamsplitters have been provided by Custom Scientific and are shown in Figure 16 and Figure 17.
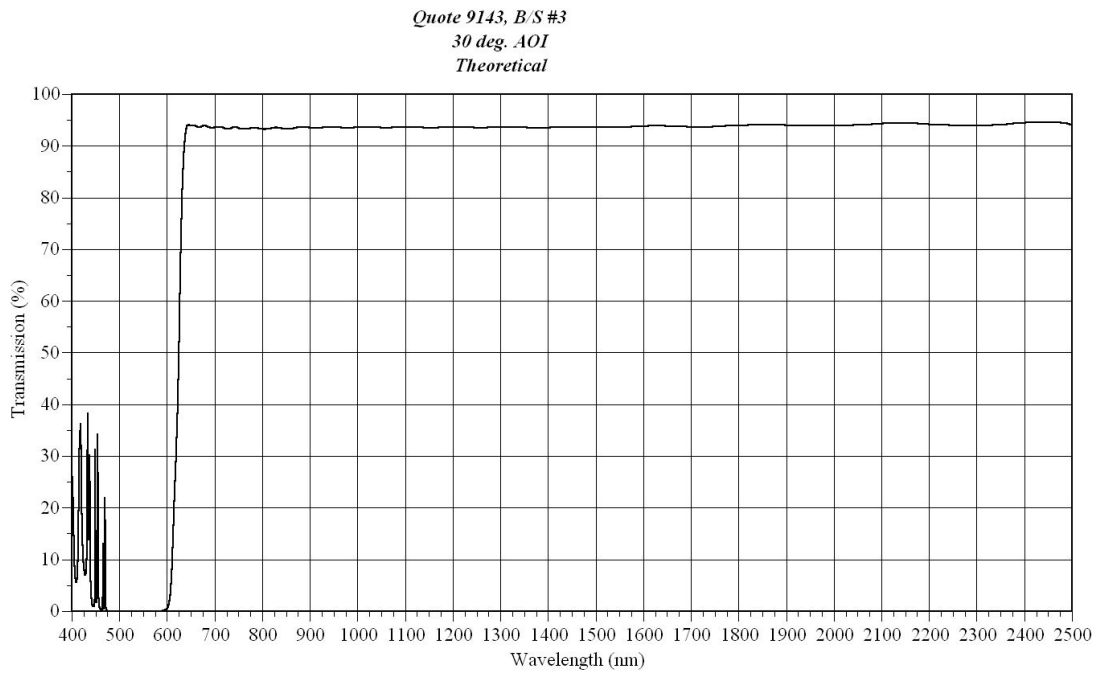
Figure 16. Theoretical transmission/reflectance curve for the wavefront sensor dicbroic during laser guide star operations.
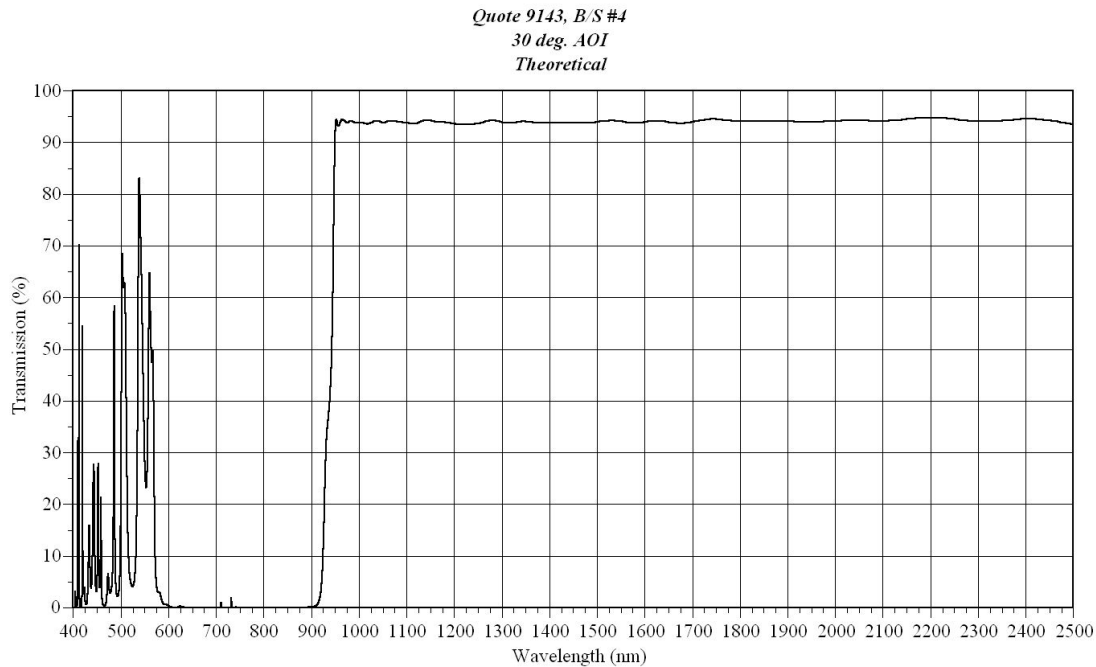
Figure 17. Theoretical transmission/reflectance curve for the wavefront sensor dichroic during natural guide star operations and IR science.

ADC

Although at this time there will not be support for visible light science with adaptive optics, it is believed that with a laser guide star upgrade, AO science in I-band will be achievable. An atmospheric dispersion compensator (ADC) will be required for observations in I-band. A preliminary design exists for an ADC on ShaneAO, but will not be implemented at this time.

Waveplate

For polarimetry the existing Lick 3m AO system employs a deployable half wave plate and Wollaston prism. The half wave plate is mounted within a rotation stage and sits outside (directly in front of) the IRCAL dewar. The Wollaston prism is contained in one of the filter wheels within IRCAL. The optics will remain in the upgraded ShaneAO system, although the cold stop will be moved upstream optically of the Wollaston in order to provide a consistent pupil for both polarizations. This will be accomplished by shifting the pupil image within IRCAL.

Wavefront Sensor

As indicated in section 7.1.4.3, the wavefront sensor pick-off is located optically downstream of both deformable mirrors. To maximize efficiency and performance at different guide star brightness levels and seeing conditions, a selection of two subaperture samplings is available, with the possibility of adding a third. The system provides the option of sampling 8x8 or 16x16 across the pupil (corresponding to 37.5 cm and 18.75 cm sampling on the primary

mirror) with the ability to upgrade to a 30x30 sampling if a laser with sufficient return flux becomes available. During initial operation with the existing Lick laser, the wavefront sensor will be operating with 8x8 subaperture sampling.

Because the pick-off to the wavefront sensor is located in collimated space, a focusing achromatic lens provides an approximately f/17.5 input into the wavefront sensor optics. Field steering will be required, especially in natural guide star mode, when the guide star may be off-axis with respect to the science object. The patrol field for guide stars is the entire 28 arcsecond diameter of the science field.

Located at the focus of the existing wavefront sensor is an adjustable iris. Currently the iris is fully open during initial alignment, and is closed to the size of a subaperture during operation to block unwanted background light. It can also used to block one of a pair of binary stars.

The current system also contains a filter wheel in the wavefront sensor path, which provides a sodium transmission filter to block unwanted light from the wavefront sensor during guide star operation, and a selection of neutral density filters which are used primarily with the existing calibration source.

Because of the different sampling requirements, three separate optical designs were developed for the wavefront sensor. To facilitate switching between the configurations, an operation that may occur several times during the night (as, for example, the observer changes from natural guide star to laser guide star observations), all three optical designs have the same length between iris and detector as depicted in Figure 18. Each of the configurations have different collimating lenses, lenslet arrays, and spot relay lenses. All three relays were designed to be achromatic between 0.6 and 0.9 microns, the wavelength range over which natural guide stars are measured. The lenses will be AR coated to maximize throughput at 0.589 nm. The parameters for the three configurations are outlined in Table 4.

Table 4. Parameters of three configurations of wavefront sensor

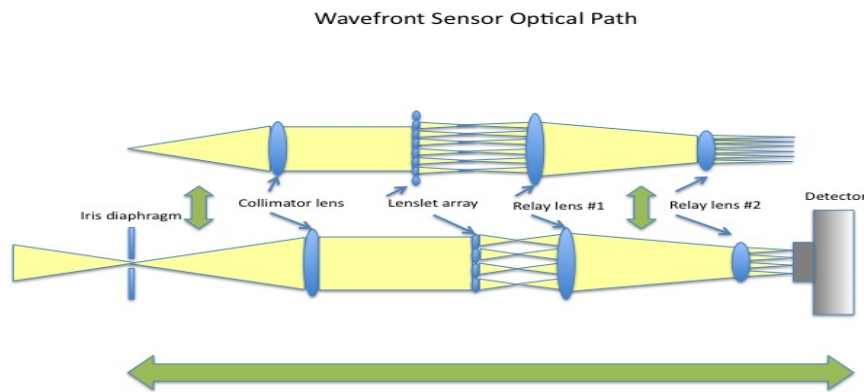| # subapertures	Pixels/subaperture	Lenslet pitch (mm)	Relay magnification	Pixel scale ("/pixel)
8	5	0.300	0.7	2.06
16	5	0.203	0.517	1.56
30	5	0.150	0.350	1.30

Figure 18. Cartoon representation of two wavefront sensor optical layouts. The two configurations are the same length between field stop and detector to simplify switching. Each of the configurations has a different collimating lens, lenslet array, and spot relay optics.

1.7.2 Science Camera Optical

Optical Design

The heart of the upgrade to the science camera will be the exchange of the 256x256 PICNIC array for a Teledyne H2RG engineering grade, with guaranteed 1k x 1k useable pixels infrared detector. The detector has 14.6 e- single CDS read (10.6 seconds), 5.25 e- Fowler-32 (340 seconds) readout. It has a quantum efficiency for wavelengths of 0.6-1.0 μm of 82%m, and a quantum efficiency for wavelengths >1.0 μm of 85%. The detector comes with a cryo-ASIC which will be incorporated into the dewar.

It was our intent to reuse as much of the existing hardware in the IRCAL dewar as possible. The optical design inside the dewar consists of an unmatched pair of off-axis aspheres with two fold mirrors for packaging. The dewar also contains an aperture wheel with a selection of slits, pinholes, an occulting finger and an open position, and two filter wheels containing a variety of bandpass filters for use in the near infrared. The filter wheels also contain two grisms – one standard grism with a resolution of about 500, and an experimental silicon grism with a resolution near 10,000. As mentioned in section 7.1.4.5 the filter wheel contains a Wollaston prism for polarimetry studies.

IRCAL was designed to be diffraction limited and sampled at K-band. Shane AO will provide diffraction-limited imaging and sampling also in J and H bands. The H2RG detector's pixels are 18 pixels, and to cover the same field of view as the current PICNIC array's 256x256 pixels requires approximately 600x600 pixels.


```
                              3D Layout
BERKELEY CAMERA
4/19/2012

                            Janos IRCAL prescription from 8-23-99.zmx
                            Configuration: All 1
```
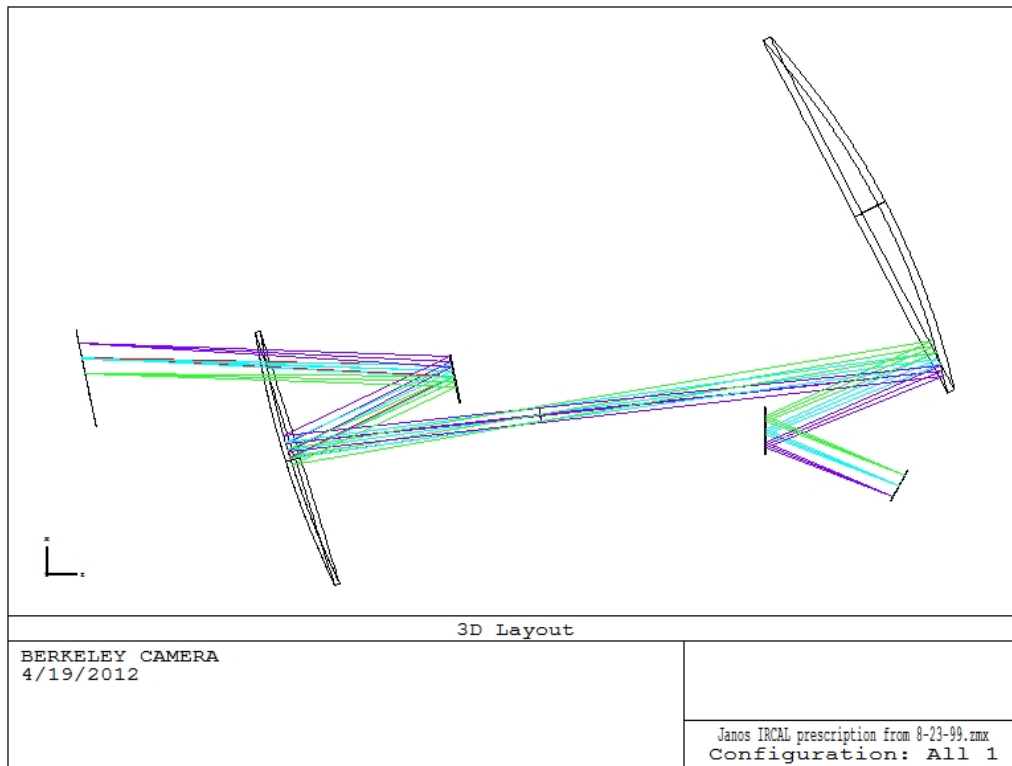
Figure 19. The IRCAL optical layout based on the Zemax file provided by IR Labs. Light enters from the AO relay to the left. The cold stop lies in the collimated space between the aspheres.
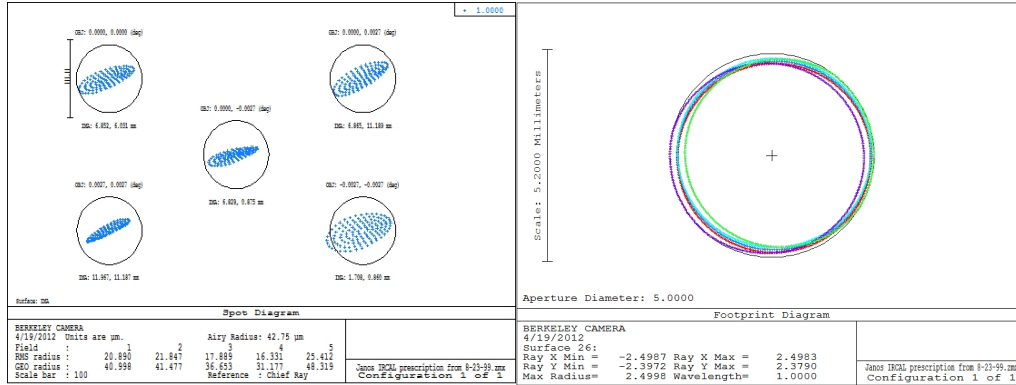
Figure 20. The Zemax report to the left shows the geometric spot analysis for the optical layout given in Figure 19. The circles represent the diffraction limit at 1 μm. The figure on the right is the footprint diagram at the cold stop. Each colored circle represents the pupil image produced by different field points.

Figure 19 shows the existing optical design based on a Zemax file provided by IR Labs. The off-axis aspheres are not configured in their optimum orientation for good imaging in the existing system, as can be seen by the spot diagram in Figure 20. Figure 20 also indicates that the pupil is either highly aberrated or tilted at the cold stop. Based on this analysis, the pupil image does not completely fill the 5 mm cold stop, so it is very possible that stray thermal emission is getting past the cold stop. It was suggested by IRCAL's designers that an upgraded optical design would ensure diffraction-limited performance at the shorter wavelengths, and we believe the high background presently seen on IRCAL could be remedied by a better analysis of the pupil image. The upgraded design has the following goals:

1. Diffraction-limited in J, H, and K.

2. Packaging that would allow the optics and new H2RG detector to fit in the existing dewar.

3. Movement of the cold stop to a position upstream of the filter wheels. This ensures a constant point spread function for both beams of the Wollaston and the entire spectrum diffracted by the grism.

The new optical design is shown in Figure 21. The pupil within IRCAL has been shifted by moving OAP4 in the 2nd relay. The OAPs are being used in their best possible configuration for imaging. The location of the focal plane allows sufficient space for the H2RG detector and ASIC.
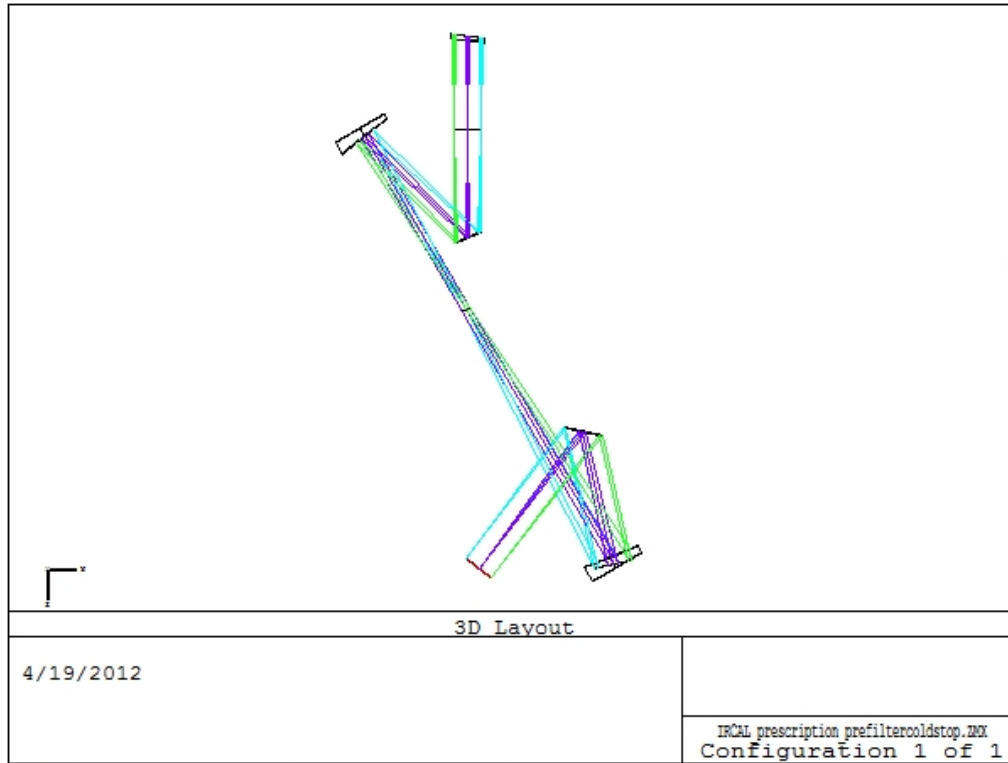
Figure 21. The new optical design for IRCAL. Light is entering from the AO relay at the top of the figure. IRCAL's tilted window can be seen as the first surface. The cold stop lies at the plane drawn in the collimated space between the two OAPs. The new fold arrangement of OAP2 and the second fold mirror allows plenty of space for the new infrared detector package.

The new AO system will allow telescope tub rotation, enabling orientation of the science object on the slit or occulting finger. As the tub rotates, the secondary support spiders will also appear to rotate as seen at the pupil image at the science camera's cold stop. In the existing system the cold stop has occluding spiders to block the secondary emission. In the upgraded system will not have these spiders since it is impractical to co-rotate the mask inside the dewar. The cold stop will still have a secondary obscuration, implemented by photo lithography on glass substrate. This of course adds two additional cold surfaces in the science path.

Optical System Performance

The science path includes the entirety of the OAP relay and the optics within the IRCAL dewar. Results of the image analysis are shown in Figure 22. The image is diffraction-limited in J-band at all points in the field-of-view. The image distortion is 1.4% over the field of view. It should be noted that the image plane at the focus of the adaptive optics relay (at the aperture stop of IRCAL) has less than a percent of distortion – the IRCAL optics are causing the majority of the image distortion. The field curvature is significant at the IRCAL focal plane, almost 0.7 mm sag, but does not cause the images at the extreme field points to become blurred beyond the diffraction limit. The wavefront error map shown in Figure 22 represents the output of the AO system, giving an on-axis wavefront error of only 3 nm peak-to-valley as designed.
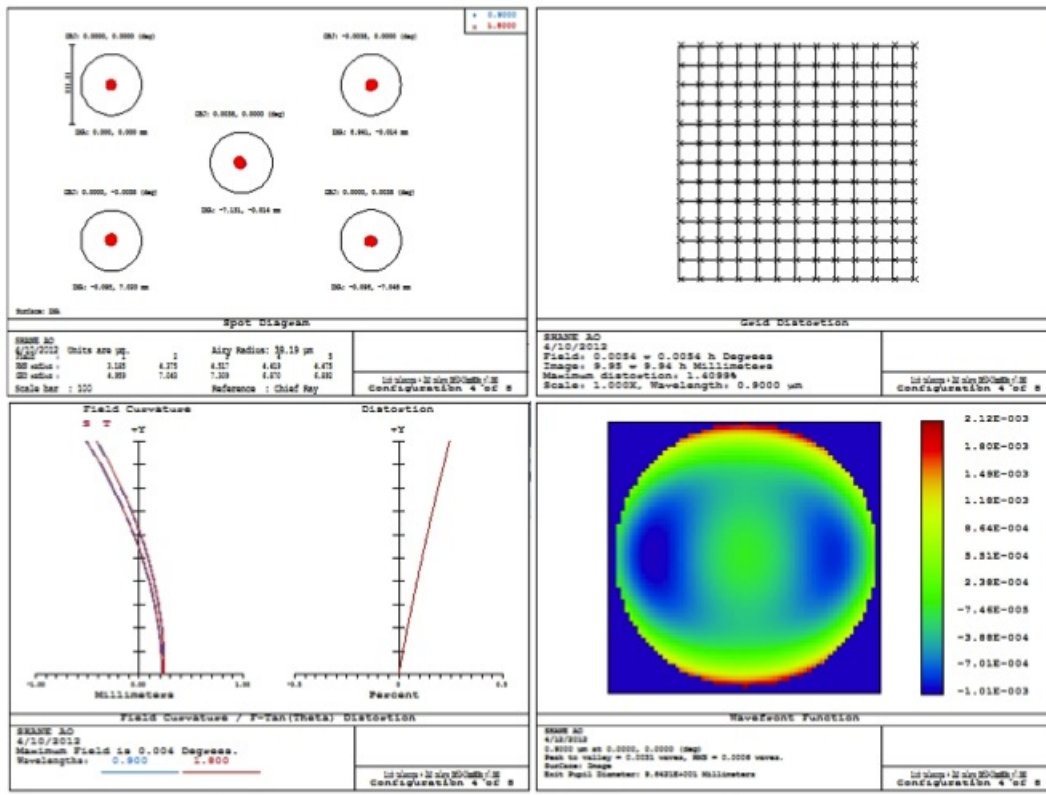
Figure 22 System performance at IRCAL detector focal plane. *Top left* shows the geometric spot diagrams for on-axis and four extreme field positions at J and K bands, well within the diffraction spot size at J-band indicated by the black circles. *Top right* displays the grid distortion map for the full 20 arcsecond field. Maximum grid distortion is 1.4%. *Bottom left* displays the field curvature and distortion. Though field curvature is present, it does not contribute significantly to degradation of the image (as seen in the spot diagram). Finally, *bottom right* shows a map of the aberrated wavefront at the focal plane, with a magnitude of approximately 5 nm peak-to-valley.

1.7.3 Tip/tilt/focus Sensor

There are several challenges in the design and performance of the focus sensor. As described in 7.1.3 the TTFS consists of only one powered optic, which scans the 120" field of view mounted to the Little Joe detector. However, the image plane provided by the adaptive optical OAP relay suffers from aberrations and field curvature which must be taken into account for the focus measurement to be valid. Figure 23 and Figure 24 demonstrate the difficulty, showing the geometric spot and field curvature analyses, respectively, of the 120" field of regard imaged by the 1st OAP relay. As one moves the TTFS detector and reimaging lens across the patrol field, the focus of the first OAP relay shifts, adding a spurious focal error signal. Having the ability to refocus the TTFS at each field position would alleviate the problem, but is mechanically difficult. To determine if the error signal can be calibrated out, a series of Fresnel propagation simulations were performed.
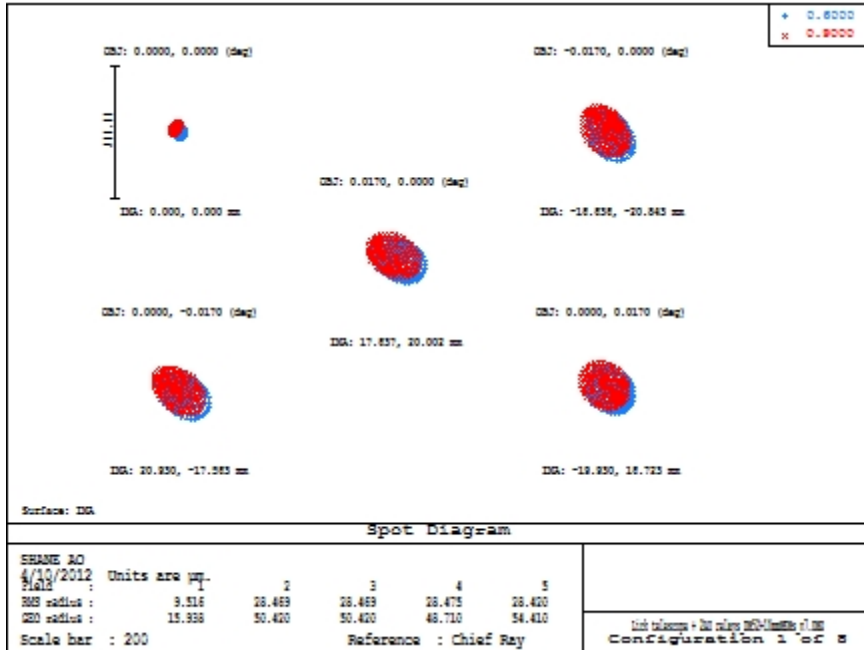
Figure 23. The geometric spot analysis at the focal plane of the first OAP relay. At the extreme field points of the 120"
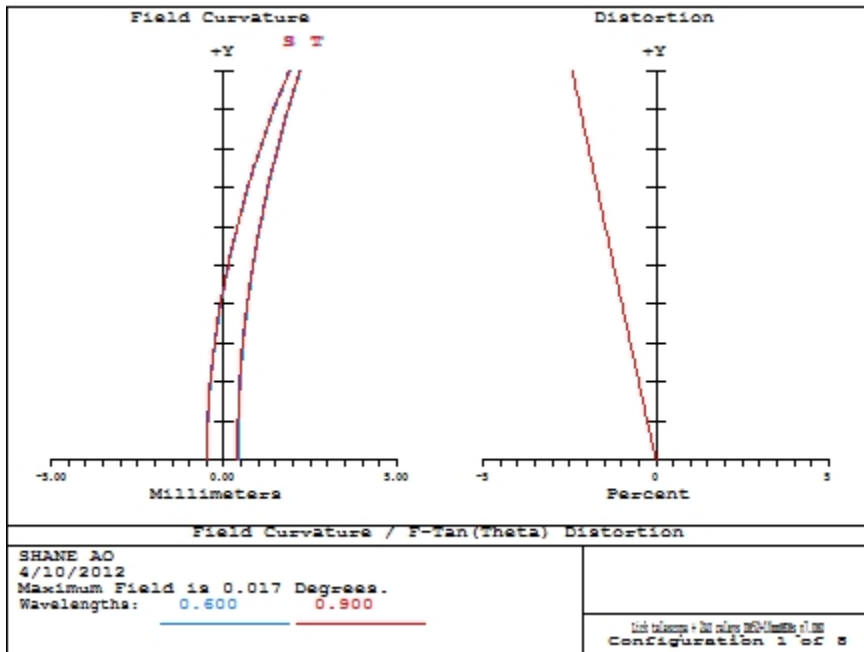field of view the image suffers from astigmatism and field curvature.

Figure 24 Analysis of the field curvature (left hand plot) at the focal plane of the first OAP relay. At extreme field
points the image focus is shifted by almost 3 mm.

The results of the Fresnel analysis are shown in Figure 25. A number of simulations were done for different amounts
of applied astigmatism (from 0.25 to 4.0 waves). As can be seen, the sensitivity of the sensor increases with increased
astigmatism, but the signal becomes non-linear at less defocus. To calibrate the effects of field curvature, the sensor
must remain in the linear signal region even with the added defocus due to field curvature. The field curvature will
introduce approximately 3 mm of defocus at the extreme field points of the 120" field. Because there is a change in

f/# between the OAP relay and the focal plane of the TTFS detector, each 1 mm of defocus at the OAP relay focal plane corresponds to 30 μm of focus shift at the Little Joe (the lateral magnification goes as the square of the paraxial magnification). It can be seen in Figure 25 that the linear regime of signal extends for a couple of millimeters, even for large amounts of applied astigmatism. Thus the field curvature can be calibrated for. As can focal shifts due to the insertion of filters before the tip/tilt/focus sensor or IRCAL. Still to be determined, however, is whether the additional astigmatism at the edges of the field can be tolerated.
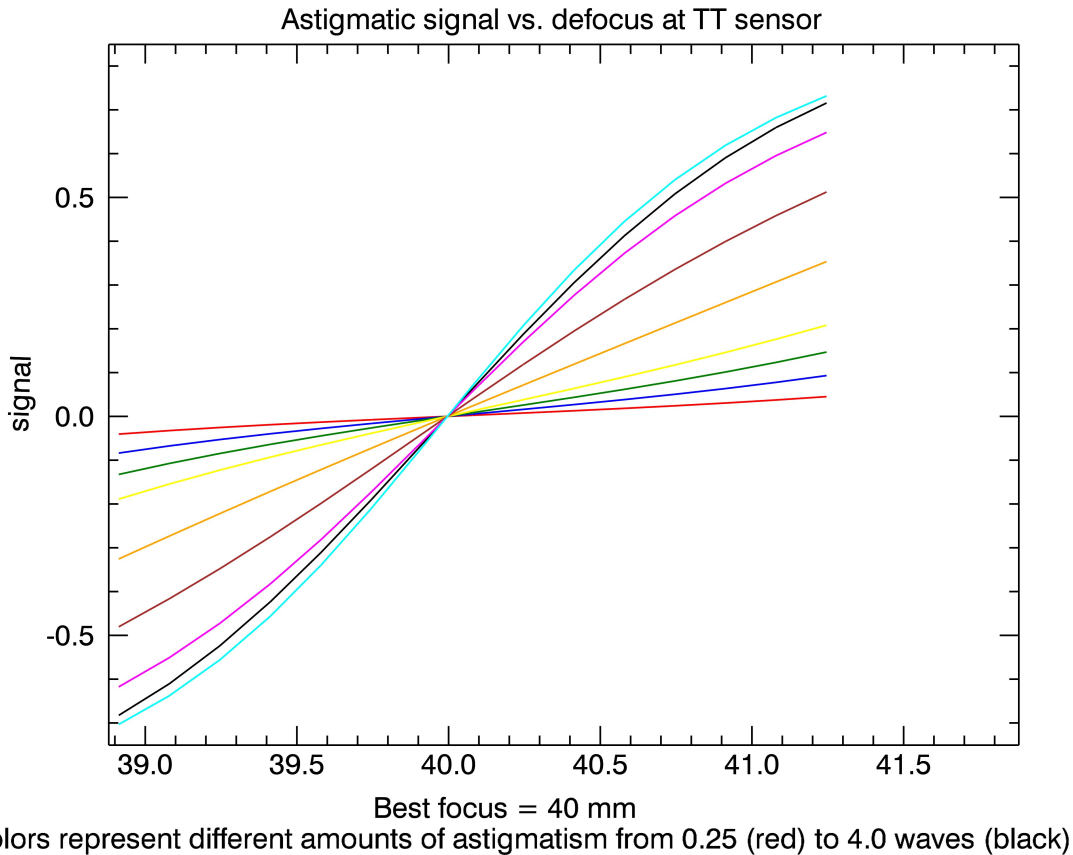

Figure 25. Fresnel propagation analysis of the astigmatic focus sensor signal versus defocus at the focal plane of the Little Joe detector. Different colors represent different amounts of applied astigmatism.

Another challenge in designing the tip/tilt/focus sensor was the broadband nature of the natural star light. The dichroic beamsplitter will transmit 0.6 – 0.9 μm light, and the broadband light must provide accurate focus measurement. The astigmatic lens has therefore been designed as an achromat. Figure 26 shows the residual chromatic focal shift for the TTFS of about 50 μm P-V. This results in Figure 27, the behavior of the defocused geometric spots for defocus values on order of a depth of focus. Depending on the color of the natural guide star, a baseline "in-focus" signal can be determined, and defocus around the baseline will be detected.
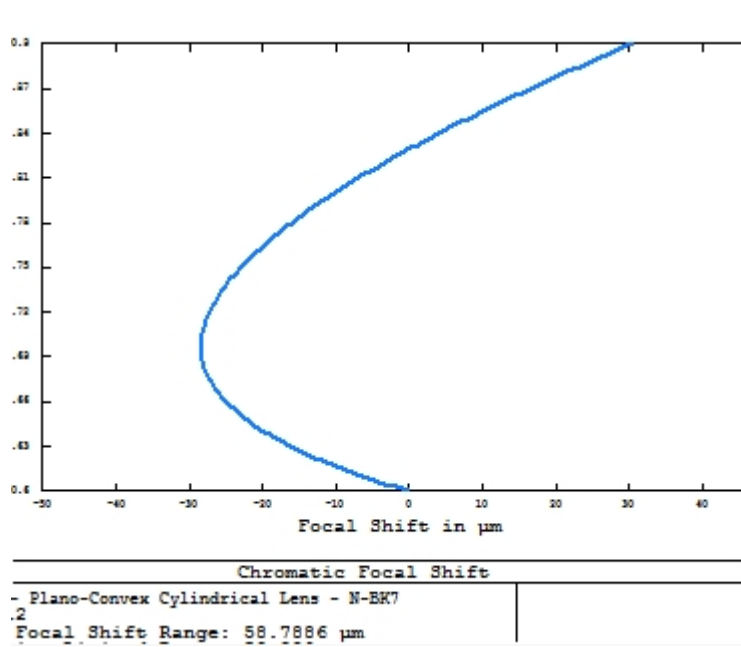
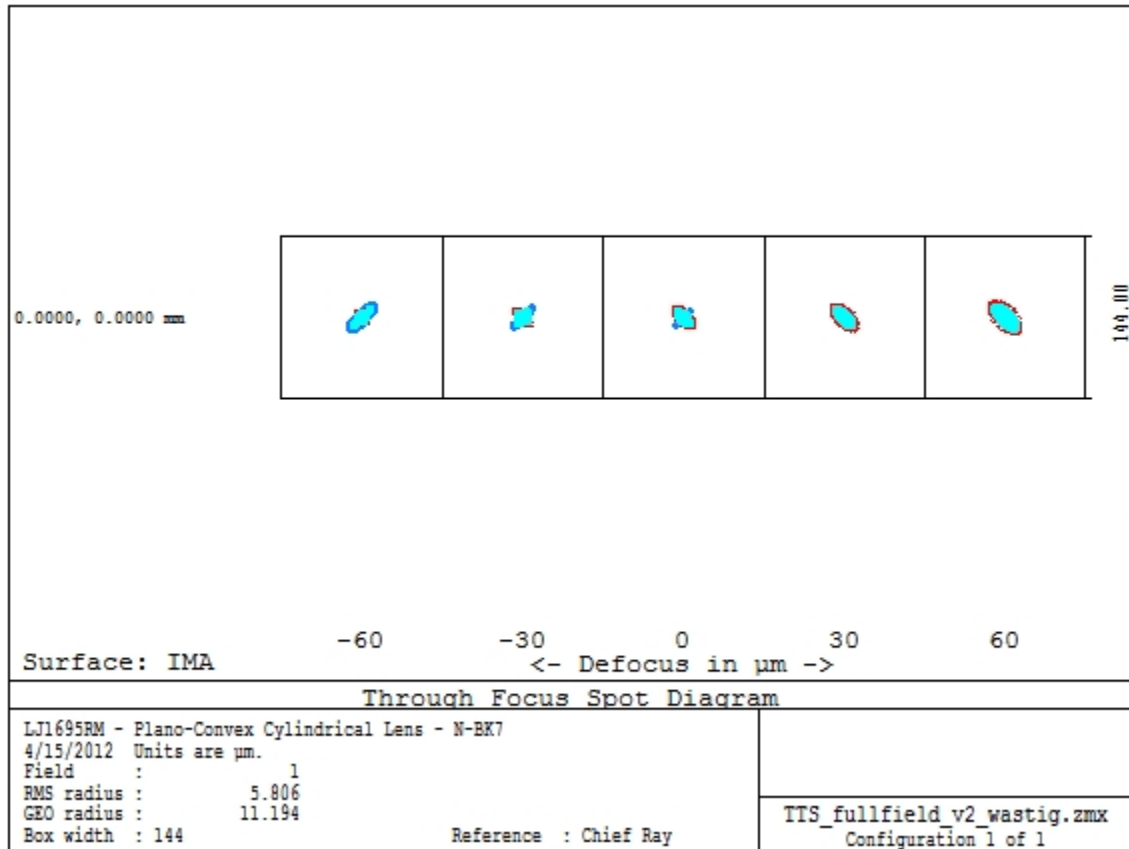Figure 26. Chromatic focal shift of astigmatic lens in TTFS.

Figure 27. TTFS spots for a focal shift on order of the depth of focus (~30 μm).

1.7.4 Wavefront Sensor Optical Path

As described in section 7.1.4.6, there will be two wavefront sensor configurations when Shane AO sees first light on the telescope, with the option to upgrade to three configurations at when laser return is sufficient. The main concern within the wavefront sensor is the performance of the optical relay between the lenslet array and the wavefront sensor detector. The lenses of the relay must provide the correct magnification to image the lenslet arrays onto the fixed subapertures of the detector. Distortion, field dependent aberrations, and chromatic aberrations should be minimized to provide a near-perfect grid of Hartmann spots on the detector.

Figure 28 and Figure 30 provide a performance analysis for the relay lenses alone for the 8x8 and 16x16 subaperture configurations, respectively. Each report plot shows the layout in the top left, geometric spot diagrams as compared to the pixel size on the Scimeasure CCID66 (box) in the top right, a distortion map on the bottom left which indicates that the distortion over the entire array of Hartmann spots is well under 0.01%, and the chromatic focal shift over the $0.589 - 0.9$ μm is about 60 μm, less than the depth of focus.

Figure 28. Analysis of the 8x8 subaperture configuration spot relay, showing layout (*top left*), geometric spot analysis for the central and outer subapertures with the scale box the size of a single wavefrtont sensor pixel (*top right*), grid distortion (*bottom left*) and chromatic focal shift (*bottom right*) over the 0.589-0.9 micron wavelength range.

Figure 29. Hartmann spots produced in Zemax when wavefront sensor model is coupled with telescope and adaptive optics system, 8x8 subaperture case.
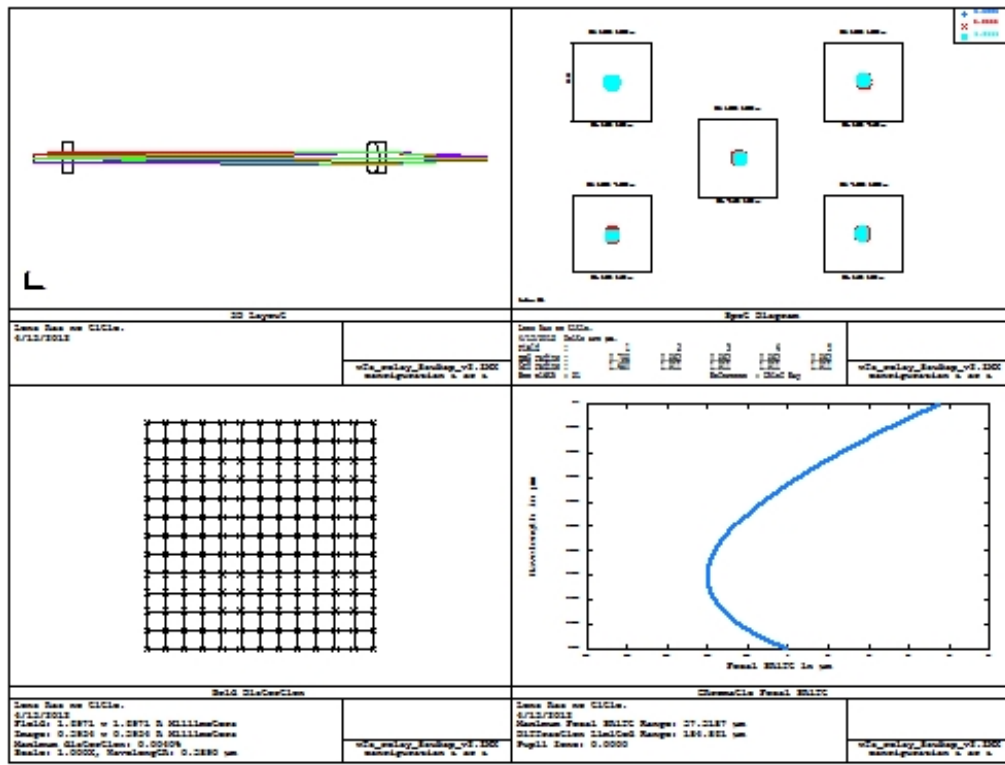

Figure 30. Analysis of the 16x16 subaperture configuration spot relay, showing layout (*top left*), geometric spot analysis for the central and outer subapertures with the scale box the size of a single wavefrtont sensor pixel (*top

right*), grid distortion (*bottom left*) and chromatic focal shift (*bottom right*) over the 0.589-0.9 micron wavelength range.
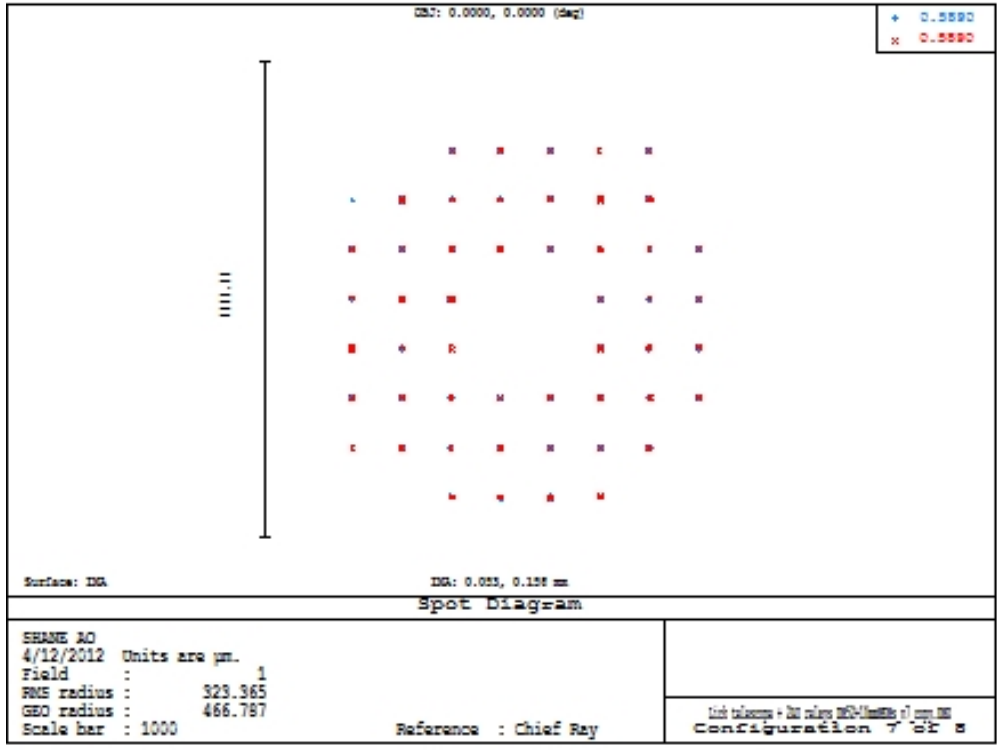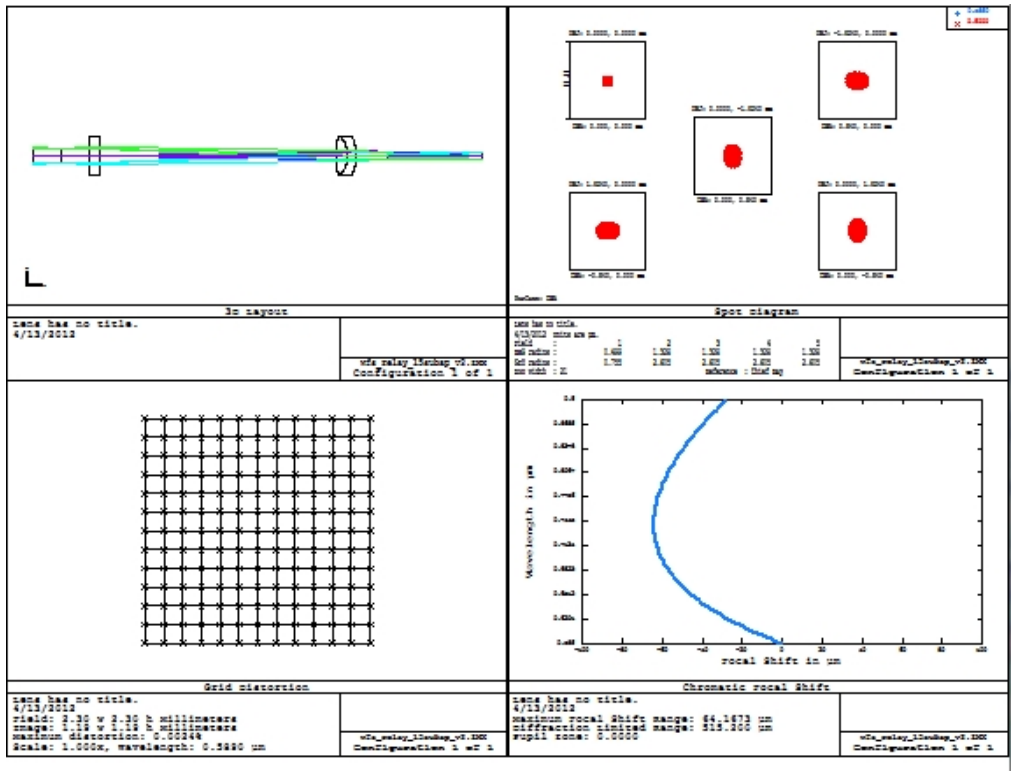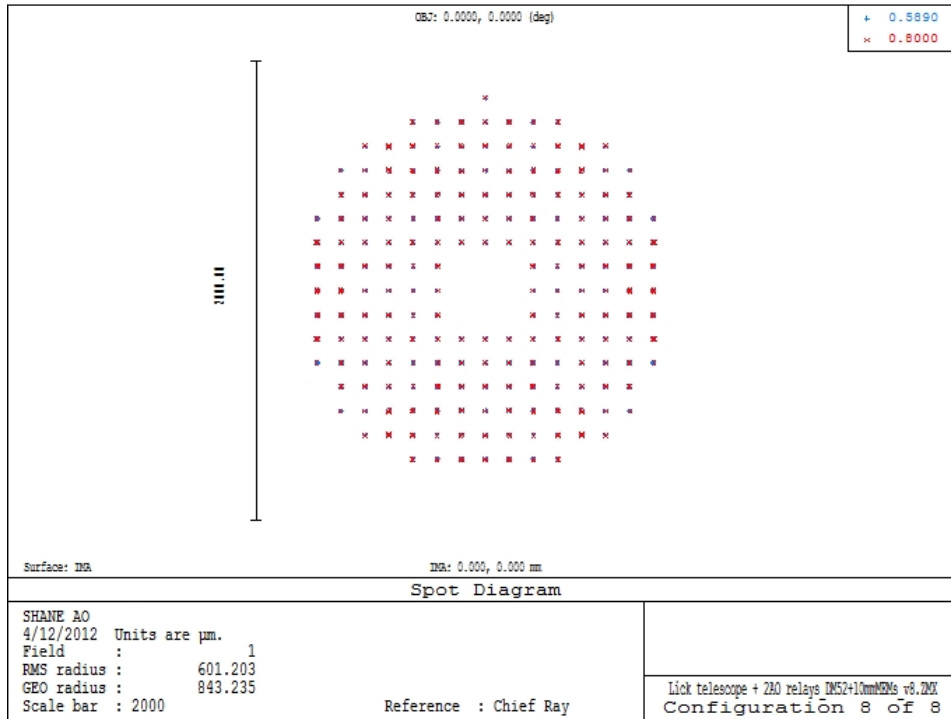

Figure 31. Hartmann spots produced in Zemax when wavefront sensor model is coupled with telescope and adaptive optics system, 16x16 subaperture case.

Figure 29 and Figure 31 show the resulting Hartmann spots on the Scimeasure wavefront sensor detector when the wavefront sensor optics is coupled with the entire AO relay and telescope in Zemax. Spot pitch is 105 μm for both configurations (four pixel subapertures plus one pixel guard band).

1.7.5 Pupil Image Analysis

Adaptive optics systems contain many surfaces which are conjugate to the entrance pupil of the telescope, and for which good pupil imaging is imperative. In ShaneAO these include both deformable mirrors, the lenslet arrays in each configuration, and the cold stop located within the IRCAL dewar.

In order to analyze the imaging of the entrance pupil, the Zemax design of the adaptive optics relay, wavefront sensors and IRCAL were set up so that the primary mirror became the object, and the telescope focus became the aperture stop with a diametr equal to the science field of view. The field points were defined as the center and outer diameter of the primary mirror.

In this mode, spot diagrams now show how a point on the primary mirror will be imaged at the surfaces conjugate to the primary. Grid distortion and field curvature plots indicate the distortion, tilt, and curvature of the pupil plane at each of the surfaces. For an adaptive optics system to provide good correction, the primary mirror should be imaged with an amount of blurring and distortion which is small compared to the scale of a subaperture or actuator. Inside the IRCAL dewar, the blurring of the pupil image will determine the amount of undersizing of the cold stop necessary to adequately block the thermal background.

Woofer DM

Figure 32. Pupil imaging on the woofer mirror. The footprint of the overlapping pupil images from on-axis and four extreme field points is shown in the *top left*, with the black circle the size of the ALPAO clear aperture *Top right* is the spot produced by five points on the primary mirror – one on-axis and four at the edge of the pupil – with a box the size of the actuator pitch of the deformable mirror. *Bottom left* indicates the distortion of the pupil image. *Bottom right* shows field curvature and distortion plots. The field curvature plot is dominated by pupil tilt.

The first pupil image in the system falls on the ALPAO woofer DM, with a 2.5 mm actuator pitch. The footprint diagram in the upper left of Figure 32 shows that extreme field points overlap at the pupil. The top right confirms this, showing spots that are very small (compared with the actuator size) for the 28" diameter science field. The grid distortion, shown in the bottom left, is 0.18%, showing little distortion of the pupil. The pupil does, however have a large amount of tilt at the woofer DM (and the tilt of the DM is unfortunately in a direction that worsens this effect). Projected on the sky, the pupil tilt is equivalent to a 136 m tilt in the plane being corrected.

Tweeter DM

Figure 33 shows the same analysis for the pupil imaged on the tweeter mirror. The footprint diagram indicates that pupils from extreme field points overlap, and show how the pupil is placed within the 32x32 actuators. The geometric spots are compared to the actuator pitch (box) of 0.340 mm. Pupil distortion on the MEMs is 0.12%, and as can be seen pupil tilt is negligible (the pupil curvature is visible in the field curvature plot and is approximately 200 μm in sag.

Figure 33. Pupil imaging on the tweeter mirror. The footprint of the overlapping pupil images from on-axis and four extreme field points is shown in the *top left*, with the black square the size of the MEMs active area. *Top right* is the spot produced by five points on the primary mirror – one on-axis and four at the edge of the pupil – with a box the size of the actuator pitch of the deformable mirror (0.340 mm). *Bottom left* indicates the distortion of the pupil image. *Bottom right* shows field curvature and distortion plots. The field curvature plot is dominated by pupil tilt.

Wavefront Sensor

Also of interest is the behavior of the pupil image on the lenslet array of the Hartmann sensor. If the pupil image is overly blurred or distorted at the lenslet array, we may not be sampling the pupil adequately. Figure 34 shows the spot diagram of the primary mirror imaged onto the lenslet array in the 8x8 configuration, and a distortion map for the pupil image. The scale bar in the spot diagram indicates the size of a single lenslet in the array. Pupil distortion on the lenslet array is only 0.12%. The 16x16 subaperture mode has very similar results. We are not making any gross errors in sampling the pupil at the lenslet array.
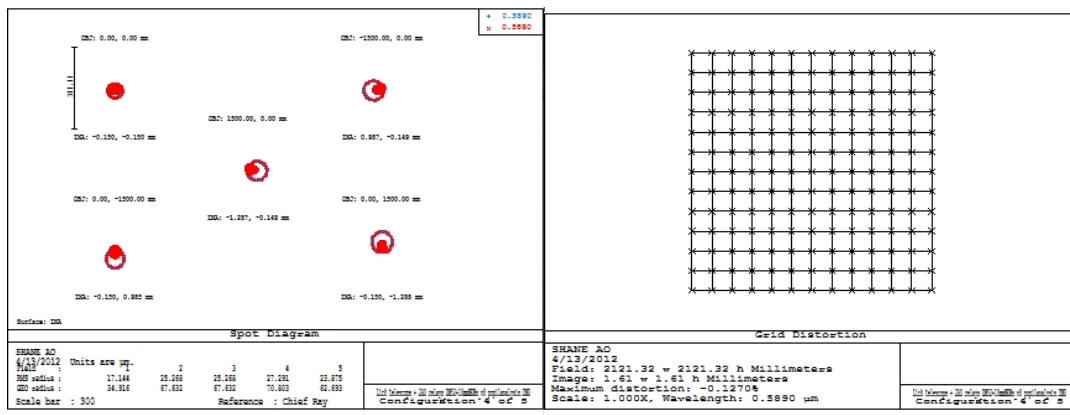

Figure 34. Pupil image quality and distortion at lenslet array for 8x8 subaperture configuration.

Science Camera Cold Stop

Figure 35 shows the behavior of the pupil at the cold stop within IRCAL. The amount which the pupil at the cold stop is aberrated, tilted or distorted determines the amount the cold stop must be undersized to avoid inadvertently letting in stray thermal light. Undersizing, however, reduces the overall throughput of the system. Upper right in Figure 35 shows that the pupils from extreme field points do not overlap exactly. This is due to the field dependent aberrations shown in the upper right (with a 100 μ scale bar) and the pupil tilt (0.3 mm over the 3.85 mm pupil) shown in the bottom right (graph on left). Distortion is small (0.1%). As a result, the cold stop will be undersized by at least 200 μm.

Figure 35. Pupil behavior at cold stop located inside the IRCAL dewar. *Upper left* is a footprint diagram showing overlapping pupils from extreme field points of the 28" diameter field of view. The pupil is approximately 3.85 mm in diameter. *Upper right* shows geometric spots produced by five points on the primary mirror – one on-axis and four and the edges – with the scale bar showing 100 μm. The *lower left* plot shows the pupil distortion, and the *lower right* gives an indication of pupil curvature or tilt, and distortion.

1.7.6 Throughput

The system throughput is evaluated in the throughput and emissivity spreadsheet (*link*).

1.7.7 Tolerancing

There are two kinds of tolerancing issues we address: The tolerances needed for the fabricated mechanical mounts and the tolerances required on manufactured optical components.

Mechanical tolerances

Detailed tolerance requirements for the mechanical design are given in the ShaneAO spreadsheet, under the "Optics List" tab. Most of the mounting tolerances are standard optical tolerances.

The most difficult requirements are the stability requirements of the mounts which are not in the common path of the tip/tilt sensor and IRCAL. Long exposures (3-4 hour) on dim objects require stability at the science camera of a tenth of a diffraction limit. Any motion seen by the tip/tilt sensor will be corrected by the tip/tilt mirror, regardless of whether it also exists in the science optical path. Thus the wavefront sensor dichroic tower, all components in the second relay, IRCAL itself, and the tip/tilt sensor have very tight stability requirements to maintain less than a tenth of a diffraction limit of image motion on the science camera. These requirements are made difficult by the changing gravity vector of Cassegrain focus and the changing temperature of the dome environment.

Another area of tight mechanical tolerances is in the wavefront sensor mounting. The lenslets and detector array grid must be registered to a small fraction of a subaperture. For the registration between the two to be on order of a tenth of a subaperture requires alignment precision of 10 μm between the lenslet array, relay lens optical axes and detector.

Optical Manufacturing tolerances

There are several custom optics in the ShaneAO system: Off-axis parabolas, dichroic beamsplitters, astigmatic lens for the tip/tilt/focus sensor and spot relay lenses for the wavefront sensor configurations. Most of the manufacturing tolerances are to typical high quality optical standards. A few parameters warranted more discussion in the sections below.

OAP Alignment Tolerance

A decenter or tilt of the off-axis parabola are both equivalent to an error in the specified off-axis distance of the parabola. A Zemax analysis shows that the image quality is not overly sensitive to small errors in the off-axis distance. Therefore the tolerance in angular and lateral position of the OAPs will be determined by the beam deviation and the resulting pupil position. Because the OAPs in each pair are aligned independently (see Section 7.2.5), the intersection point of their collimated beams determines the position of the deformable mirrors. Any angular error will shift the deformable mirror away from the pupil.

Errors in the DM position were calculated for both relays given angular errors of 0.01° and 0.1° for each of the four OAPs. Each of the relays was evaluated separately. Results of this analysis are displayed in Table 5.

Table 5. Results of OAP angular error tolerance analysis.

Angular error	Error in woofer position, bench (mm)	Error in MEMs position, bench (mm)	Error in woofer position, sky (m)	Error in MEMs position, sky (m)
0.01°	0.09	0.05	3.5	2
0.1°	0.9	0.5	35	19.5

1.7.8 Dichroic beamsplitters' reflectance

To maximize the return of the laser guide star, we have specified reflectances of >99.5% at 0.589 μm for both the TTFS dichroic and the LGS wavefront sensor dichroic.

1.7.9 Wavefront sensor relay lens

The magnification of the spot relay in the wavefront sensors is very sensitive to the focal length of the second relay lens. Their radii of curvature therefore have a specified manufacturing tolerance of 0.2%.

Mechanical Construction and Layout

Mounting to Telescope

The adaptive optics components are mounted on a single optical table which is mounted to the telescope at the Cassegrain focus. The system is removable for regular instrument change operations at the observatory. The mount interface is the standard one at the Cassegrain ring, which allows field rotation angle to be set using the tub rotator. This enables the entire AO system to be set at an arbitrary field angle on an object-by-object basis, which is useful for example to set the spectroscopic slit angle on the sky (there is no other means of rotating the slit).

The AO optical line is co-aligned with the telescope line by adjusting the first steering mirror. This, along with pointing the telescope, puts a star at a given field position and centers the AO pupils to the telescope pupil.

1.7.10 Opto-mechanics

3-D renditions of the optomechanical system are provided in an e-drawing file *(KT link)*. The free reader for e-drawings is available *here*. Figure 36 shows one projective view.

The optomechanical system is required to hold the optical alignment to tolerances needed for long-exposure diffraction-limited imaging. Since the instrument is Cassegrain mounted, the optical mounts are subject to changing gravity conditions. Key points in the system have been designed to prevent drift of alignment due to both gravity and temperature.

The most difficult objective is long (3-4 hour) exposure on dim objects using the laser guidestar and a off-axis tip/tilt star. In this case, the tip/tilt sensor must remain co-registered to the science detector to much less than the diffraction-limit for the duration of the exposure. Even if the infrared director is read out periodically to avoid background saturation, we assume there is no field star on the science detector frame to act as a position reference for co-registering frames, therefore the system must remain stable on the sky for the total exposure duration. In spectroscopic observing, the co-registration requirement can be relaxed somewhat to some fraction of the slit width.

In natural guidestar observing, the guidestar is bright enough for wavefront sensing and it is within the science field of view, so its image on the science detector can be used for co-registering many short exposure frames. Nevertheless, the system has been designed so that the wavefront sensor remains stable with respect to the science detector over at least one hour exposures.
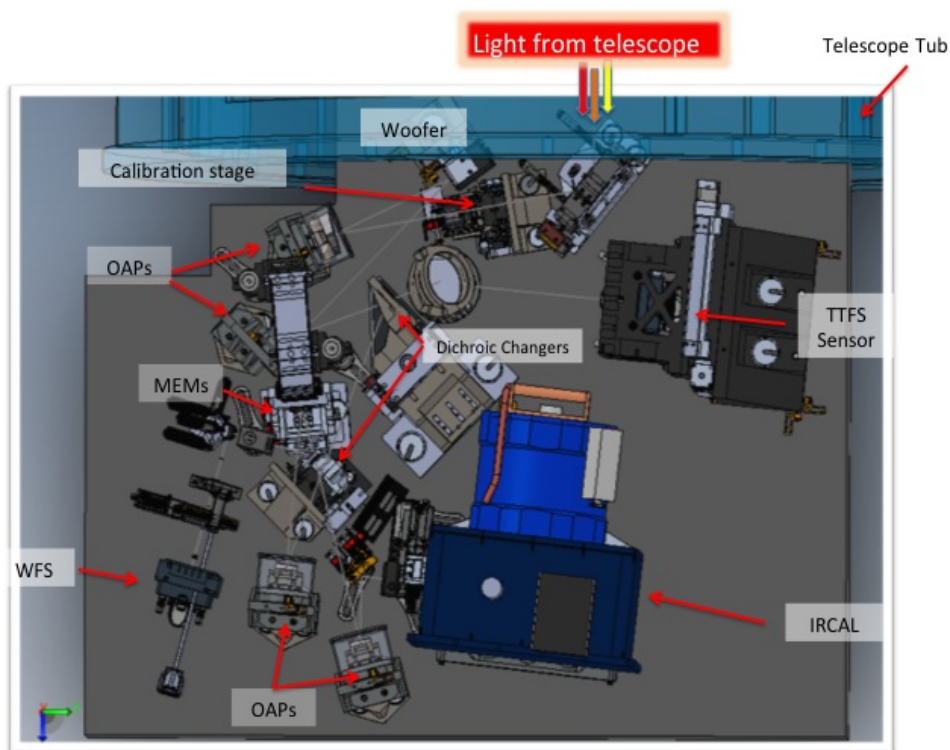
Figure 36. ShaneAO optics bench populated with mounts, mounted underneath the TUB of the 3-meter telescope. The optical path is shown in light grey. Major components are labeled.

The ShaneAO optical bench will be mounted to the Lick 3-meter telescope's tub (Figure 36), and Cassegrain focus will be located after the first fold mirror of the AO system. The Calibration insertion stage is located at Cassegrain focus. The following sections will describe specific subsystems of the Shane AO optical bench. The flexure and temperature analysis results will also be explained.

Stages and Mounts

Calibration Stage

As described in section 7.1.2.1, ShaneAO will have two fiber calibration sources and an acquisition camera located at the Cassegrain focus. The mount for these optical devices is shown in Figure 37. The mount must have the ability to position each of the fiber sources or the Flea acquisition camera on the optical axis, or remove them entirely from the beam. It must also be able to adjust the position of the fibers in a direction parallel or perpendicular to the optical bench. This motion is achieved through use of a THK stage coupled to a servo motor in the y-direction (perpendicular to the bench) and a New Focus picomotor for fine adjustments in the x-direction (parallel to the bench). Both axes are load encoded. The THK linear stage must travel through a hole in the optical bench to completely clear the beam during normal operation.
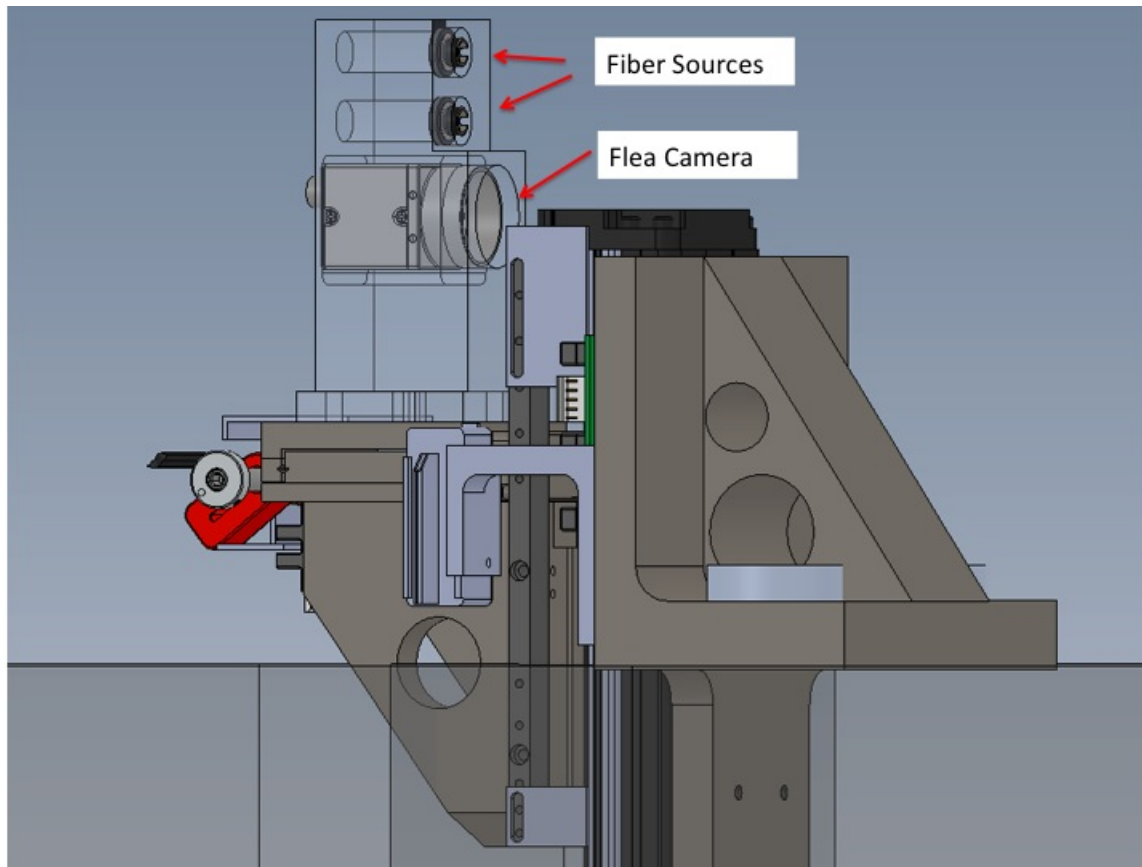

Figure 37. Calibration stage containing a white light fiber source, a laser source, and a Point Grey Flea acquisition camera. A linear stage allows selection of any of the three optical devices, or their removal from the beam. The stage is mounted through a hole in the optical bench allowing for the 100 mm of linear travel.

Off-axis Parabolic Mirror Mounting

It was decided for stability to use fixed mounts, without unnecessary degrees of freedom, wherever possible. Though this often requires more effort during the alignment of the instrument, we believe it results in a more robust and stable design. The four off-axis parabolas (OAPs) will thus be mounted as shown in Figure 38. The hexapod bases of the mount provide stability against the changing gravity of the optical bench during observations. The optic is supported by three tabs attached to the edge. The mount provides for clocking adjustment and locking, and pucks threaded into the base provide adjustment for tip/tilt and height. The lateral position of the mounts will be done with nudgers which

may remain on the table as a reference for repositioning. Each of the mirrors has a cylindrical cover for protection from hands, tools, and dust, the base of which can be removed when the OAP is needed for use.

Figure 38. Mount used for all four off-axis parabolas.

Woofer DM Mount

The low-order woofer DM (section 7.1.2.3) will be mounted with the same philosophy as stated in section 7.2.3.2, minimizing degrees of freedom for the sake of stability. The mount is shown in Figure 39. The low-order mirror has a 2.5 mm pitch between actuators, so it's absolute alignment with respect to the wavefront sensor and tweeter mirrors is not as critical as it would be for a mirror with smaller pitch. All of the adjustments, including height, tip and tilt of the mirror, as well as lateral position of the base, are made with nudgers (shown in yellow).

Figure 39. The mount for the ALPAO DM52 woofer deformable mirror.

Tip/tilt Dichroic Changer

Downstream from OAP2 is a dichroic changer in the converging beam, providing a dichroic beamsplitter or flat mirror as described in section 7.1.3. These are large optics, 3 inches in diameter, to accommodate the 120" field of regard for the natural tip/tilt star. The mount is required to be extremely stable, because any motion of the mount will be evident on the science camera as image motion, but will not be sensed on the tip/tilt sensor (which works in transmission through the dichroic).

We have thus set a stability requirement which keeps the science image steady to one tenth of a diffraction limit over a three hour exposure. This corresponds to an angular stability of 2 arcseconds over three hours on the dichroic changer, which is experiencing a varying gravity vector during the exposure as the telescope tracks.

The mount is shown in Figure 40. Because the optics are large in diameter, the linear stage travels through a hole in the optical bench, with the servo motor located below the bench. Three apertures are present to receive a flat mirror for NGS operation, and a choice of dichroic beamsplitters to accommodate NIR science and an eventual upgrade to visible light science.

Figure 40. The tip/tilt dichroic changer.

A flexure analysis was done to assure that this mount had adequate stability. The analysis included the effects of "Hertzian" deflection of the ball bearings in the stage. The results of the analysis are shown in Figure 41. Both the mount and carriage were were modeled, giving 1.9 arcseconds flexure during a 3 hour exposure (telescope starting at zenith and transversing to 45 degrees off zenith). Thermal distortion of the mount will be primarily in the x-y plane perpendicular to the beam axis, and should have little effect on deflection of the optical beam.
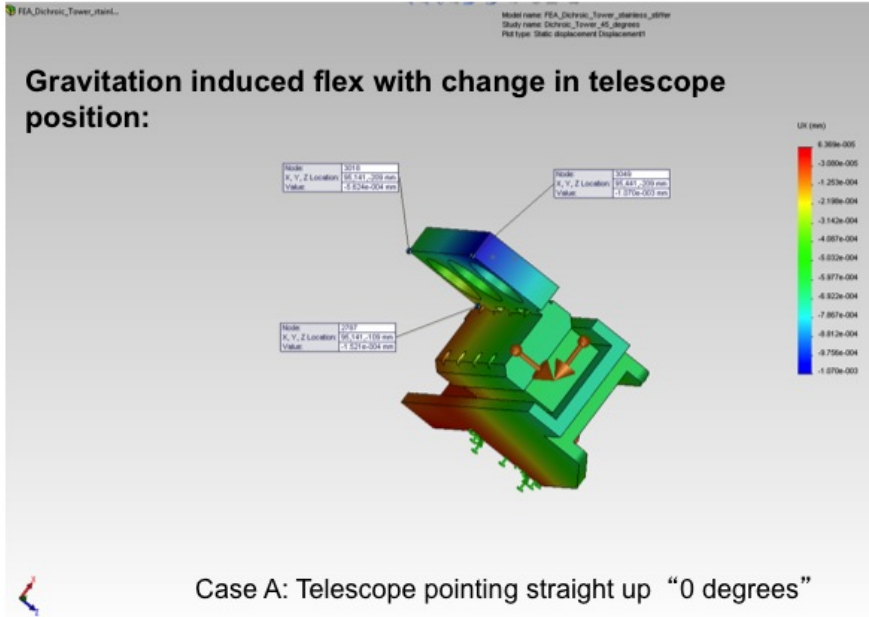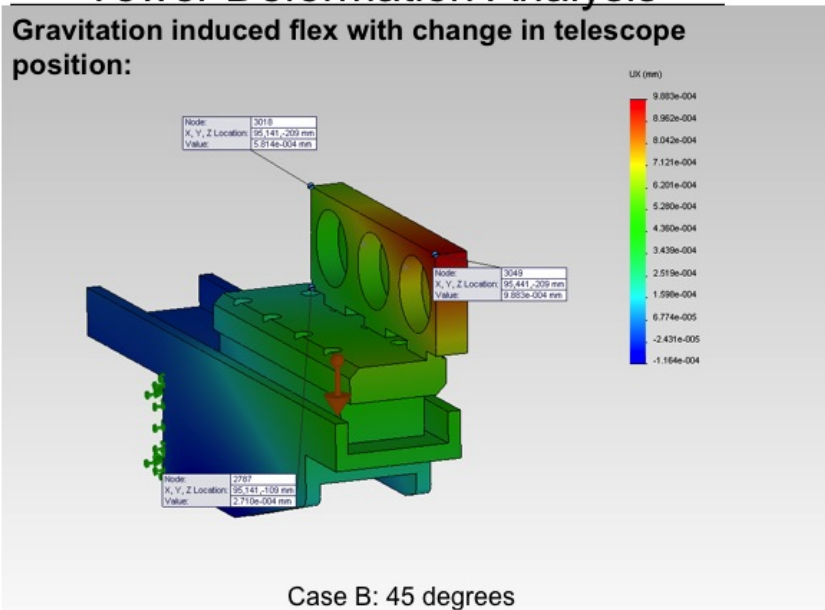
Figure 41. FEA analysis of the tip/tilt dichroic changer deformation due to a changing gravity vector over a three hour exposure.

Figure 42. Periscope for directing the beam to the tip/tilt/focus sensor. This mount is stationary.

Periscope Mount

The converging beam coming off of OAP2 to the tip/tilt sensor requires a slight redirection to avoid interference with the calibration stage and the first fold mirror. A pair of fixed periscope flat mirrors directs the beam down towards the table and away from the first fold mirror. The mount for these mirrors is shown in Figure 42.

The bulk of the mount will be fabricated in one piece by 3-d drawing "printing" process that involves sintering, which is fusing powdered bronze and stainless steel alloy at high temperatures.

Tip/tilt/focus Sensor Linear Stage

To select a tip/tilt/focus reference star from the 120" field of regard, the Little Joe camera and the achromatic/astigmatic focusing lens are translated on a x-y stage. The required motion is ± 32 mm travel in x and y to cover the entire field of regard. The stability requirement for a 3 hour exposure time is less than 2.5 μ, the angular displacement is less than 1 arcminute. The focusing lens must be held securely to the detector, with a lateral displacement between the two of less than a micron. The tip/tilt sensor also has a filter wheel for filters used with bright guide stars that must be mounted on the translation stage.
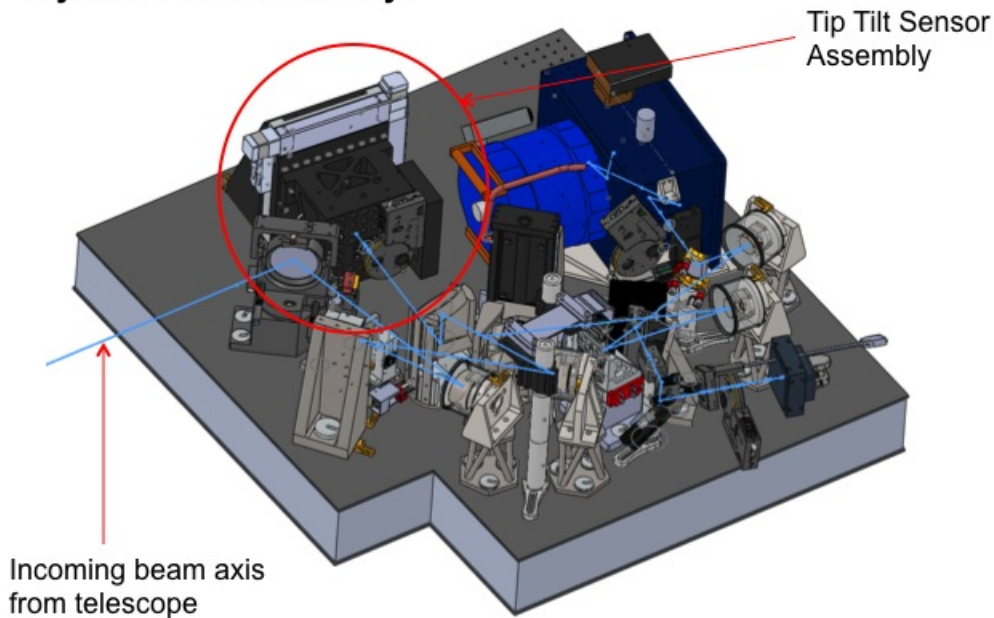
Figure 43. Tip/tilt sensor identified in main optical layout.
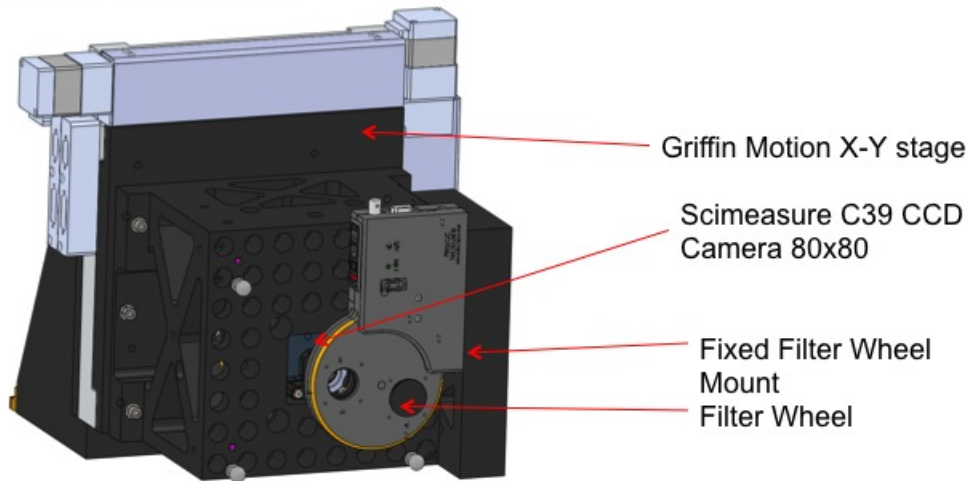
Figure 44. Complete tip/tilt sensor assembly.

Tweeter DM Mount

To properly register the tweeter DM's actuator grid to the wavefront sensor subaperture grid requires the mount have precise motion adjustability in x and y. The tweeter mount will also be adjustable in tip/tilt angles, so it can be used to fine-align pointing into the science dewar during assembly and any time the science camera is remounted after being removed for servicing.

Similar to the tip/tilt dichroic, the stability of the tweeter mount is critical for long exposure LGS operations. Any residual motion at the plane of the tweeter is not sensed by the tip/tilt sensor, resulting in uncorrected image motion at the science camera.

The MEMs mount design is shown in Figure 45. The mount is based on a stock New Focus 9082 kinematic stage, which has all the needed degress of freedom.
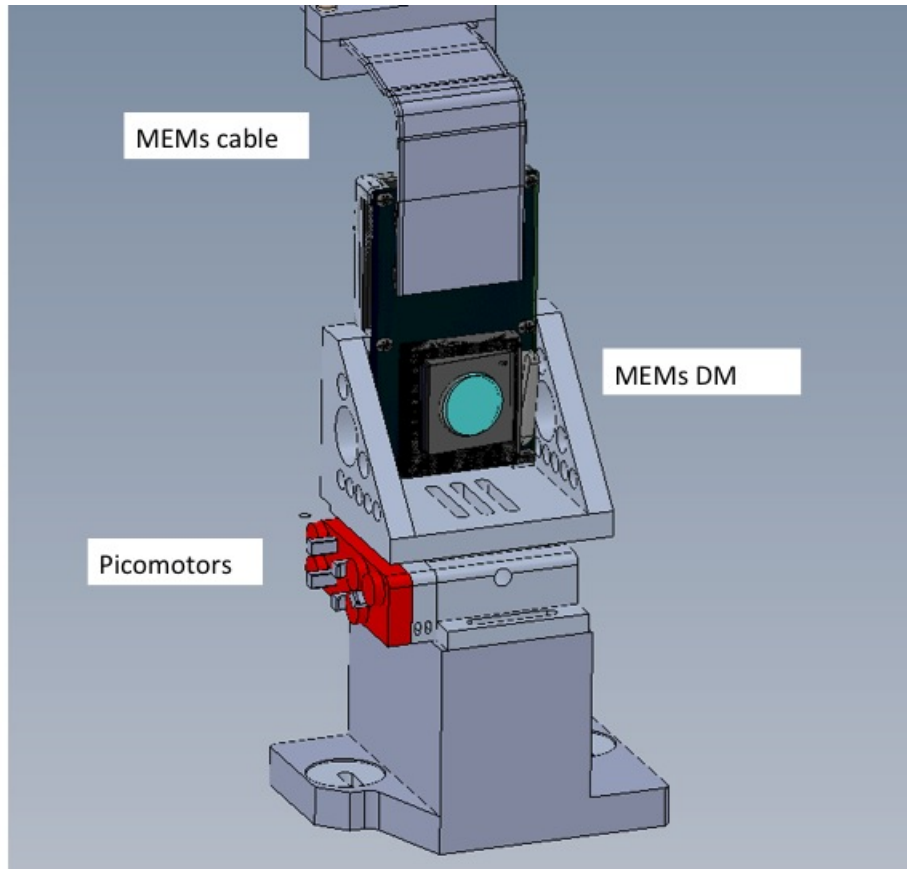
Figure 45. The ShaneAO MEMs mount. The picomotors provide precise motion in x, y, z, tilt x and tilt y. The cable is directed out the top of the mount and is strain relieved before curving around the optical bench to the electronis.

Initial finite element analysis indicated that the deflection of the mount during a 3 hour exposure would somewhat exceeded our stated 2 arcsecond absolute stability requirement. Laboratory tests with a purchased stage revealed that most of the deflection is within the stage, traceable to the indentation of spherical kinematic supports into an aluminum plate. To bring this back into spec, we are making modifications to the stage: stronger springs (within load of picomotors), refabricated base plate using a hardened material and/or sapphire disks inserted to minimize brineling by the kinematic balls. We performed additional laboratory tests using M2 tool steel plate and more preloading. These tests confirmed increased stability such that it will meet the specs.

Wavefront Sensor Dichroic Changer

The WFS dichroic changer provides a choice of two dichroics (described in section 7.1.4.3) depending on whether the system is being used in laser or natural guide star modes. The stability requirement is not so great on the WFS dichroic mount as for the tip/tilt/focus sensor dichroic. When the system is used in laser guide star mode, the wavefront sensor tip/tilt signal is used only to stabilize the laser guide star through the steering mirror in the laser launch telescope. During natural guide star operation, the science objects are typically the guide object itself, and is therefore not dim enough to require a 3 hour exposure. We have thus shortened the stability requirement to 2 arcseconds stability over a 30 minute exposure. The field of regard for the wavefront sensor in the second relay is only the 28 arcsecond diameter science field, This leads to significantly smaller beamsplitters, and therefore less load for the gravity vector to act upon. The mount is shown in Figure 46.

Figure 46. The wavefront sensor dichroic changer. The diameter of the optics is one inch. Linear travel of the changer dictates that the stage be mounted through a hold in the table.

The geometry of the mount results from the geometry of the surrounding optical beams – this is a very tight space

optically (see Figure 47). FEA analysis indicates that the mount easily meets the stability requirements. Most of the deflection is due to the angular deflection of the linear bearings.
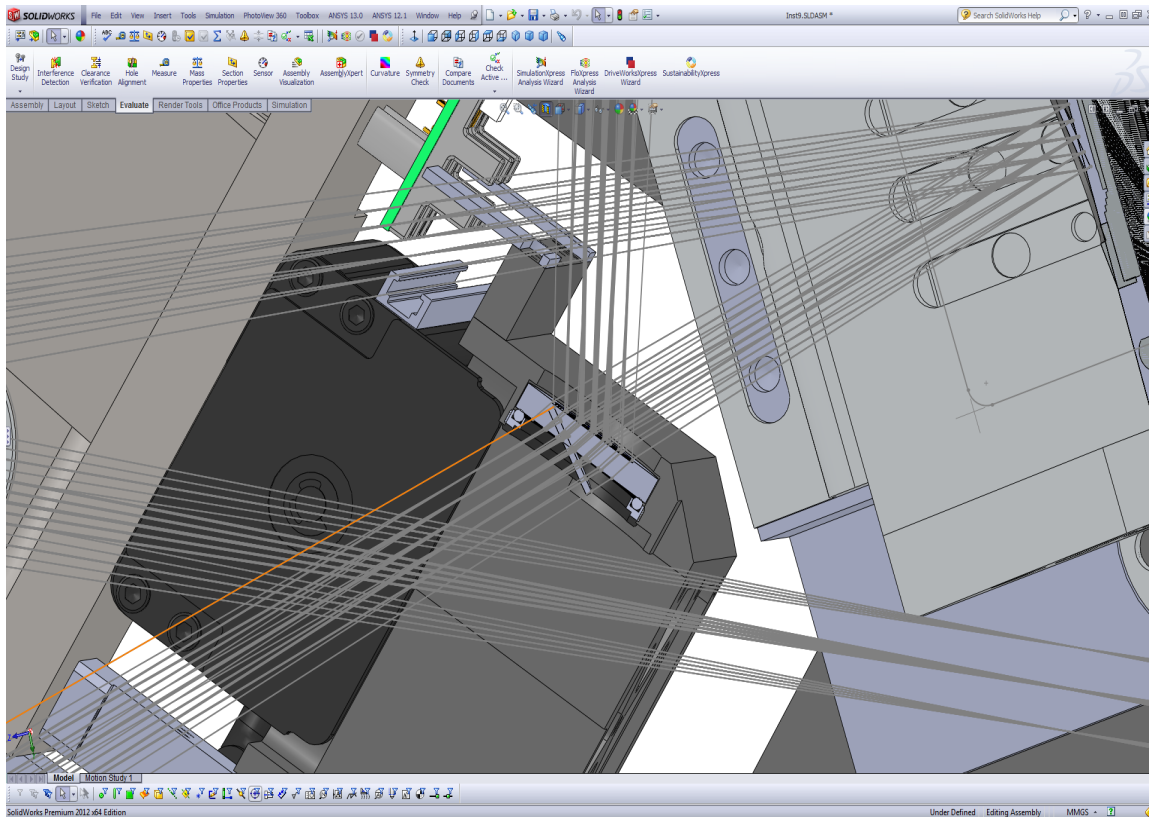

Figure 47. Beam geometry around WFS dichroic changer dictates the geometry of the mount. The wavefront sensor dichroic is shown near the center of the image. The light enters the second relay from the bottom right. The MEMs resides at the top right. The wavefront sensor optical path continues out the top of the image.

WFS Mounting

The mechanical mounting of the wavefront sensor has some special requirements for degrees of freedom. During a typical night of observations, the adaptive optics system will switch modes from NGS to LGS and possibly back to NGS again as morning approaches. In the upgraded AO system, LGS will work with the 16x16 (or possibly 32x32 mode) while NGS will typically be operating at 8x8. Switching between the two modes easily is desired. The entire wavefront sensor package, from field stop to detector, must be mounted on a focus stage to adjust for the changing distance to the sodium layer as the telescope changes pointing, and to refocus for natural guide star operation.

There are also several alignment requirements both within the WFS and between the WFS and the rest of the AO relay which require special mechanical features. For example, it is necessary that the lenslet array be rotationally adjusted so that the grid of lenslets matches the grid of pixels. The relay lenses must be adjusted in the z-direction (along the optical axis) to give the proper magnification to match the lenslet pitch to the subaperture pitch. The lenslet array must be placed at the proper distance from the collimating lens to be conjugate to the telescope primary. An adjustable field stop at the front end of the wavefront sensor allows calibration and alignment of the wavefront sensor optics (with the field stop closed down enough to create a point source at the input of the WFS), masking of Rayleigh light or close binaries, and masking of ghosts or stray light (with the field stop set at the size of the subaperture, 6 arcseconds). The grid of the lenslet array/detector subapertures must be aligned with the grid of MEMs actuators in the AO relay.

The WFS mount shown in Figure 48 meets all of these requirements. The bottom linear stage provides focus adjustment for the entire wavefront sensor package. The linear stage perpendicular to the bottom stage allows changing

between two (with room for an upgrade to three) subaperture modes. Each of the three optical relays sits in v-grooves that travel perpendicular to the optical axis to center the relay between the iris and detector. The iris is a motorized, adjustable iris that can close down completely. The Scimeasure "Big Joe" wavefront sensor camera is mounted within a flexure mount and can move small amounts in the x and y directions through the adjustment of New Focus picomotors to align the detector with the lenslet array. The entire package is mounted on feet that allow adjustment in height and tip/tilt, and nudgers provide adjustment in x (parallel to the bench) to allow alignment with the MEMs grid.

Figure 48 The Shane AO WFS mechanical package.

Science Camera Mount

The Science Camera dewar is referred to as "IRCAL" in this discussion. Even though the science camera optical design differs from that of the original IRCAL, we are re-using the dewar, so the mechanical issues of dimension and weight are identical.

To increase the stability of the AO system it was decided to hard-mount the IRCAL dewar to the optical bench (presently the dewar sits atop a linear focusing stage). The design approach was to have a plate permanently mounted on the optical bench to which the dewar kinematically attaches. The base plate is made of steel to behave identically to temperature changes as the steel optical bench. IRCAL's shell is aluminum, so the bracket attached to IRCAL is also aluminum. The kinematic points between the bracket and the base plate allow differing thermal deformation without causing stress.

IRCAL's mounting design allows for easy installation and removal. When the bench is vertical, IRCAL can be placed on the bottom kinematics and it will not move or slip while the top securing screw is installed. Two more lock down screws than come in from the bottom of the dewar. The IRCAL mounting arrangement is shown in Figure 49.
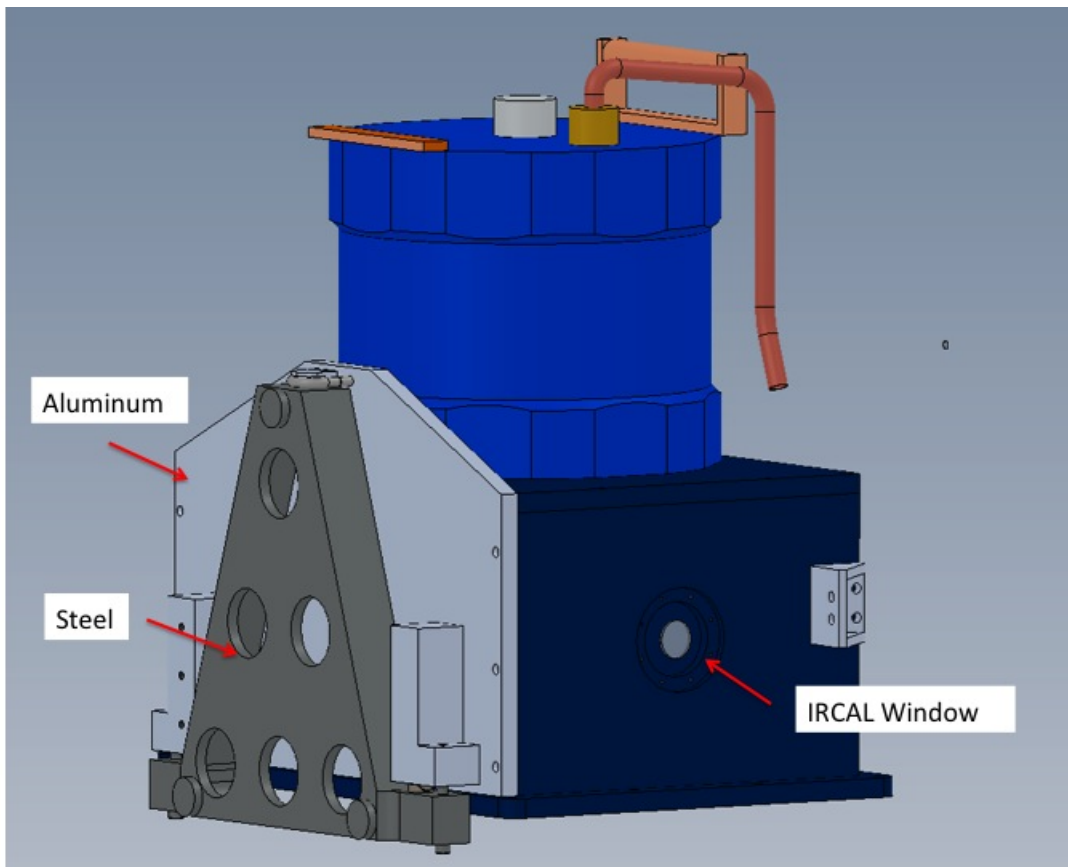

Figure 49. The IRCAL dewar (dark and light blue) in its mounting arrangement. The steel plate will be permanently

fixed to the optical bench, the aluminum bracket will be permanently fixed to IRCAL, and the two plates will couple kinematically.

Stability Analyses

Gravity-induced Motion Analysis

Because Shane AO is a Cassegrain mounted instrument, the gravity vector will change during observations. To meet Shane AO's tight stability requirement, the mechanical system is designed so that the optical system alignment is maintained within tolerance over a range of gravity angles. The flow down to deflection of individual components on the optical bench is given in the *ShaneAO summary spreadsheet*, "Optics List" tab.

A finite element analysis was performed on several of the more critical optical mounts, as well as on the complete system of AO optical bench and science camera dewar. The results are summarized in Table 6.

Table 6. Deflection due to gravity.

Object	Change in gravity vector (degrees)	Maximum Linear Deflection (μm)	angular deflection (arcsec)	angular deflection requirement from ShaneAO spreadsheet
Breadboard, loaded, TTFS vs IRCAL	45	25.26	1.96	
OAP mounts	90	1.163	2	10" over 45 deg
Woofer	180	0.6	0.7	10" over 45 deg
TTFS Dichroic Tower	45		1.87	2" over 45 deg
TTFS	45	1.9		3.2 microns ov 45
MEMs	45	2.1		2" over 3 hours
WFS dichroic tower	45	0.1	0.1	4" over 0.5 hr
IRCAL	45	29		3.5 microns wrt TTFS over 3 hrs

The major flexure issue is deformation of the optical table by the load of the infrared dewar. The dewar move on the order of 25 microns, where we require a diffraction-limit/10 motion, which is approximately 2.8 microns in the f/28.5 space. We understand this deflection to be an elastic, and therefore repeatable deformation, and it will be tested using a flexure test stand during integration and test phase. The present plan is to use a lookup table driven control of the tip/tilt stage to pre-compensate.

The finite element analysis results are summarized in the *ShaneAO summary spreadsheet*, "FEA" tabs.

Thermally-induced Motion Analysis

Thermal deformation analysis was also performed. There are currently no provisions for thermal control on Shane AO, therefore temperature swings of several °C are possible during a night. Ambient temperature changes will both distort the surface of the optical bench and change the height of the optical components based on their material. Most of the optical mounts are fabricated with steel, and will therefore deform uniformly. The IRCAL dewar is made entirely of aluminum, thus we will see a relative thermal deformation between science camera focal plane and the tip/tilt sensor focal plane, which is important to control to a tolerance that is acceptable for the long exposure LGS operation requirements.

Most of the mounts in the AO relay and the table are made of 304 series stainless steel, with a thermal coefficient of approximately 17 parts per million per degree C. One of the mounts, the periscope mount which is composed of bronze-steel alloy, has a coefficient of 13. The OAP bases are made of carbon steel (for better flexure stiffness) has a coefficient of 15. The infrared camera dewar is made of 6061T6 aluminum with a coefficient of 22.

The resulting thermal deformation analysis is present in the *ShaneAO summary spreadsheet*, "Thermal Deformation" tab. The biggest change is due to the contraction of the table, but there also a height changes of the critical non-common path items: tip/tilt beam path of 2 microns per degree C, and the IRCAL dewar away from the optical bench of 4.2 microns per degree C. The differential motion of 2.2 microns/degree C with a 2 degree temperature change will exceed the stability requirement of 3 microns in the non-common path. So a temperature change larger than this over the duration of a long exposure will need to be mitigated using a temperature lookup table.

Opto-mechanical Alignment Process During Assembly

To properly align the Shane AO system will require some standard alignment hardware, including an alignment laser (collimated beam), alignment telescope, several reflecting spheres (or one on a kinematic mount that can be placed in different positions), and several pairs of alignment crosshairs or pins (or a set of both) also mounted with kinematics for easy repositioning. A commercial coordinate measurement machine will be utilized to initially place the fiducials on the breadboard. The alignment can then proceed as explained in the following section. Refer to Figure 50 for placement of fiducials.

n
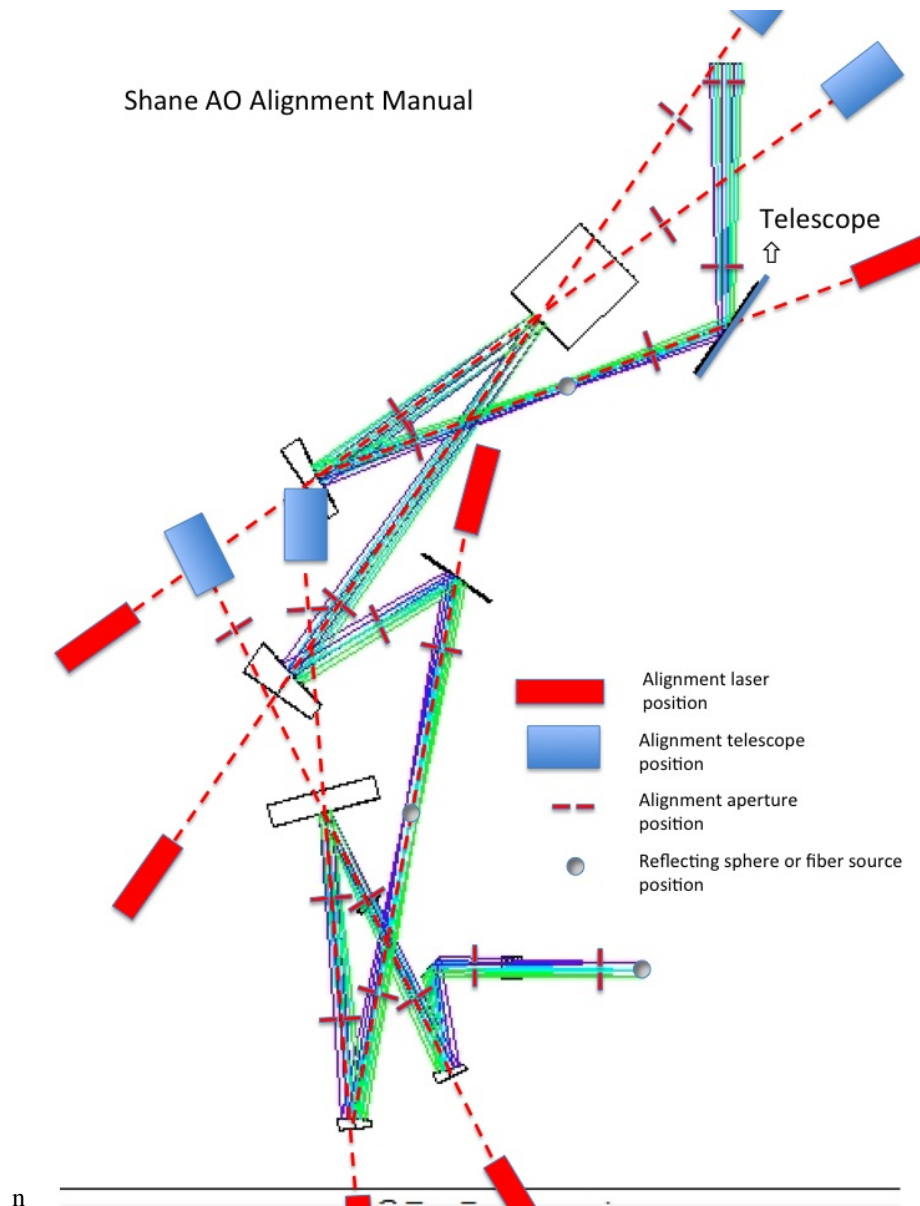
Figure 50 Reference image showing placement of fiducials, alignment lasers, and alignment telescopes in Shane AO.

Clocking of all OAPs should be fixed before installing in the AO relay. The alignment will proceed from IRCAL and work backwards through the optical system. The alignment is of course an iterative process. As one degree of freedom is adjusted, the others should be rechecked.

1. (a) (a) Second Relay (first four slides)

   (a) Define the beamlines from IRCAL, backwards towards FM2, and from OAP4 to the MEMs DM. The alignment pins (or crosshairs) can be placed with the coordinate measurement machine (slide 2).

   (b) Retro-reflect alignment laser off back of OAP4 (slide 3).

   (c) Set alignment telescope along beam line, behind MEMs position, pointing towards face of OAP4.

   (d) There should be a reflecting sphere placed at the focus of OAP4 (without FM2 in place). Adjust z-position of OAP4 until reflecting sphere is one focal length away.

   (e) Place FM2 so alignment laser from IRCAL is centered and adjust angle until beam is aligned with fiducials

between the MEMs position and OAP4.

   (f) Place reflecting sphere at IRCAL focus, make sure it's centered and projected to infinity as seen by the alignment telescope behind the MEMs position

   (g) Set alignment laser along MEMs-OAP3 beamline from position behind OAP3 (slide 4).

   (h) Place OAP3 and retroreflect off back to set angle.

   (i) With reflecting sphere at input focus of 2nd relay, use an alignment laser to set z-position of OAP3.

2. First Relay

   (a) With alignment laser set along woofer-OAP2 beamline, retroreflect off back of OAP2 to set angle.

   (b) With alignment telescope (behind woofer position) reflecting off of OAP2, use reflecting sphere (placed by coordinate measuring machine) set at OAP2 focus to adjust z-position of OAP2.

   (c) Using alignment telescope (and/or alignment laser), place dichroic tower (with mirror in position) so that reflecting sphere at input of 2nd relay is centered and one focal length away from OAP2. This will ensure that the output focus of the 1st relay is the same as the input focus to the 2nd.

   (d) Move dichroic tower to dichroic position and adjust dichroic until reflected light is following same path as for mirror (reflecting sphere is centered and one focal length away). Depending on reflectance of beamsplitter at visible wavelengths, this may be difficult with alignment telescope, and laser will be used.

   (e) Set alignment laser along OAP1-woofer beamline, and then retroreflect off back of OAP1 to set angle on OAP1.

   (f) Retroreflect off of reflecting sphere placed at telescope focus, and adjust z-position of OAP1 until it lies one focal length away from telescope focus.

3. Deformable Mirrors

   (a) Starting near the IRCAL focus, set up alignment laser in reverse direction through 2nd relay.

   (b) Set up a second alignment laser going forward through the 2nd relay, along beam path between 1st and 2nd relays.

   (c) And intersection between two alignment lasers is the tweeter position.

   (d) Adjust angle and position of tweeter until both beams overlap.

   (e) A flat mirror may be used in place of the tweeter (on same mount) for calibration, if desired.

   (f) Keeping alignment laser at IRCAL, place 2nd alignment laser on input beamline to OAP1.

   (g) Place woofer (or flat) at intersection of two beams.

   (h) Adjust angle on woofer until the two beams overlap.

4. Wavefront sensor

   (a) With alignment laser still positioned behind FM1 position, define the beamline for the wavefront sensor.

   (b) Place the WFS dichroic tower and adjust angle until beam going down defined WFS beamline fiducials.

   (c) Swithcing between dichroic beamsplitters should not change pointing – adjust beamsplitters in tower until both beams take identical paths.

   (d) Place WFS field steering mirrors, centered on beam, and pointing through center of WFS iris and mounted WFS detector.

   (e) Moving WFS detector/iris in focus should not change the position of alignment beam on detector.

   (f) Place re-imaging lens in the beam path, making sure there is no beam deflection.

   (g) Pre-aligned WFS lens tubes can now be installed.

5. Tip/tilt/focus sensor

   (a) Align TTFS lens and sensor independent of bench.

   (b) With alignment laser still located at the front end of the 1st relay, and with the TT dichroic in position, install the periscope and center the Little Joe sensor on beamline.

   (c) Install alignment telescope in place of alignment laser at input of 1st relay.

   (d) Install gage block and align perpendicular to beam with alignment telescope.

   (e) With a LVDT dial indicator probe touching the block,, translate the TTFS sensor along its range of travel making sure that it's travel is always co-planar with the gage block.

6. Calibration Stage

   (a) With alignment laser or alignment telescope in place at input of the 1st relay (still no FM1 in place), position calibration stage with all fixtures removed from beam path (stage in "open" position).

   (b) Move red fiber mount into place, verify centering with alignment laser or telescope.

   (c) Move white light fiber mount into place (without fiber installed). Verify centering with alignment laser or telescope.

   (d) Move Flea camera into place, and verify centering on beamline.

   (e) Install fibers and verify back focus.

   (f) Adjust TTFS and WFS iris to best focus positions.

7. IRCAL

   (a) Place IRCAL baseplate and IRCAL on bench. Use nudgers on baseplate to position IRCAL in approximate position.

   (b) Center beam going through IRCAL (using alignment telescope for pupil alignment and calibration source for image alignment) using the MEMs for pointing and FM2 for centering.

8. Telescope simulator

   (a) Telescope simulator will be available in the lab, with an exit pupil identical to the Lick 3-meter.

9. Align to telescope or telescope simulator

   (a) Align star image on Flea (calibration stage) by adjust telescope pointing.

   (b) Adjust focus on Flea by adjusting telescope focus.

   (c) Adjust pupil centering on wavefront sensor with FM1 (assuming WFS field steering mirrors are centered).

10. Pupil alignment- should be done with alignment telescope in lab.

    (a) With telescope simulator, one can place a point source at the entrance pupil and confirm that each of the deformable mirrors and the cold stop are conjugate to the pupil.

11. Waveplate – should be done with alignment telescope in lab.

    (a) Insert waveplate stage and verify that waveplate is centered on beam.

    (b) Insert Wollaston prism in IRCAL (located in 2nd filter wheel).

    (c) Place polarizer at output of telescope simulator to feed AO system with polarized light (may want to place immediately in front of waveplate). Rotate polarizer to minimize intensity in one beam from Wollaston and maximize other.

    (d) Rotate waveplate and take intensity readings from both beams at several positions.

(e) The position at the midpoint between the spots being alternately minimum and maximum is the angle at which the half waveplate axis is at 45 degrees to the Wollaston axis.

1.7.11 Software

1. Power Sequencing

    (a) Computers

        i. Servers (i.e. motor)

        ii. RTC

    (b) Monitors

    (c) Sensors

        i. Temp. sensor on Science Camera (before science camera)

    (d) Cameras

        i. WFS

        ii. LTT

        iii. Science

        iv. Acquisition?

    (e) Motors

    (f) Light sources

        i. Calibration

            A. Red light

            B. White light

    (g) Laser safety system – not on Pulizzi

    (h) LGS – has own Pulizzi.

2. AO System Control

    (a) AO Motor Control

        i. Tracking

            A. First fold mirror

        2 axis

1. LTT steering mirror #1

    2 axis

    Coordinated move with LTT SM #2

1. LTT steering mirror #2

    2 axis

    Coordinated move with LTT SM #1

1. WFS steering mirror #1

2 axis

Coordinated move with WFS SM #2

1. WFS steering mirror #2

    2 axis

    Coordinated move with WFS SM #1

1. WFS focus control

    Focus position of LGS changes with zenith distance.

1. Non-tracking

    (a) MEMs mount

    5 axis, probably only two computer controlled.

1. Calibration Source stage

    4 positions: red light fiber, white light fiber, open, Flea camera for alignment

1. LTT dichroic changer

    3 position: 2 LTT dichroics, depending on wavelength of science wavelength, and open

1. WFS dichroic changer

    3 positions: 3 WFS dichroics depending on LGS/WFS and science wavelength

1. Last fold mirror

    2 axis

1. WFS Iris

    Controls size of iris at focus of WFS

1. Logging

2. Telemetry Data Display

3. UI

    (a) Target submission list

        i. Send email to telescope user to request target list

        ii. Web-based form for submission of targets.

    (b) Skycat implementation

    (c) Loop parameters

        i. AO update rate

        ii. AO gain

        iii. AO integrator gain

        iv. NGS TT gain

        v. NGS TT rate

        vi. LTT gain

        vii. LTT rate

    (d) Loop Control

        i. LGS or NGS mode

       ii. AO Loop toggle

      iii. NGS TT Loop toggle

      iv. LTT loop toggle

       v. Open All loops

      vi. Close All loops

     vii. Telemetry dada collection

(e) LTT

        i. Display intensities

(f) Power Control

(g) Motor Status and Control

        i. Manual moves

(h) LTT Pointing and Centering

        i. Manual move

       ii. "Back on Axis" – zeroes pointing

      iii. "Go To Zero" - zeroes both pointing and centering

      iv. display motor position

       v. reset position numbers

(i) LGS Pointing and Centering

        i. Manual move

       ii. "Back on axis" zeroes pointing

      iii. "Go to Zero" zeroes pointing and centering

      iv. Displays position

       v. Reset position numbers

(j) Logging

(k) AO Diagnostics

        i. Display centroids

       ii. Display intensities

      iii. Display actuator voltages

         A. Woofer

         B. Tweeter

      iv. Best shape on woofer to give highest Strehl

       v. Best shape on tweeter to give highest Strehl

      vi. Flatten woofer

     vii. Flatten tweeter

    viii. r_0

      ix. PSF calculator

      x. Performance prediction calculator

          A. **Given seeing conditions, sodium column densities, mag** field, TT brightness and position, science target zernith angle, time of observation predicts Shrehl.

          B. Calculate signal to noise with exposure time, throughput.

      xi. **Ghosting check? (right now ghost image in WFS , always must** check to make sure not guiding on ghost).

  (l) Hartmann Sliders for Image sharpening

4. Configuration and Scripting

  (a) Target Acquisition

  (b) Background subtraction.

  (c) **Open-loop compensation of flexure of telescope with respect to** laser launch telescope.

  (d) Focus sensing.

  (e) Prevention of lock on Rayleigh light.

  (f) Set AO rates and gains automatically.

1. IRCAL Instrument Control

  (a) IRCAL motor control

      i. Aperture wheel

      ii. Filter wheel #1

      iii. Filter wheel #2

      iv. Communications with motor controllers "problematic"?

  (b) UI

      i. Exposure configuration

          A. Total integration time (units of frames or ms)

          B. Number of reads

          C. Number of coadds to sum into a frame

          D. Number of exposures at this setting

          E. Enter object name

          F. Display frame/exposure number

          G. Pause

          H. Resume

          I. Stop

          J. Show disk status

          K. Show detector temperature.

          L. Save all reads button (good for engineering).

      ii. Expert mode for configuring detector.

      iii. Exposure palette

        A. **On current system, retains a number of exposure** configurations to take darks, etc that match exposure.

   iv. Image display

        A. Allow image display with IDL.

        B. Ircal image displayed automatically as read in.

        C. Zoom function.

        D. Coordinates displayed in arcseconds and pixels

        E. Subtract image button.

 (c) AO system and telescope control (communications) functions

   i. User laser shutdown monitor to prevent exposure

   ii. Control telescope/wfs loops for nodding.

   iii. **Offset telescope without wfs loop control (currently on system,** but disliked). Confusing interface. Need some way to open loops and move telescope, but this needs redesign.

 (d) Image Diagnostics

   i. Strehl Tool

   ii. Noise check – sometimes IRCAL noise high, requires reset.

 (e) Logging

 (f) Configuration and Scripting

   i. Image sharpening.

   ii. Nod+wfs steering

2. AO Real Time Control

3. IRCAL Detector Readout Control

4. Laser System

 (a) Laser Clearinghouse communications

   i. **Once target list submitted via web-form, convert into** appropriate format for Space Command PRM submission

        A. **Allow for stationary pointings (boresights) in Alt/Az units** for engineering.

        B. **Submit start and stop lasing times based on 12 degree** twilight information (current lasing window 10pm to 5am).

   ii. Automatically email to laser clearinghouse.

   iii. **Receive PAM files via email and process into proper format for** laser shutdown monityor.

        A. **LCH often sends updated PAM files – allow for efficient** mechanism for rerunning data and alerting staff of updated list.

 (b) **Laser Shutdown monitor (currently connected to IRCALui but should** be made stand-alone). Desired improvements:

   i. **Enhanced interface to select appropriate target list based on** telescope position.

   ii. **Graphical tools to help observers select targets based on** zenith distance, hour angle, and laser shutdown times and durations.

  iii. **Warning that telescope position doesn't match position of the** currently selected laser shutdown file (and possible hardware lock to prevent laser shutter from opening).

 iv. Automate laser shutdown for satellites.

  A. Does not rely on laser operator or slow software.

Operating Environment

From the perspective of the user, observing operations are performed totally from computer terminals. The user interface must properly reflect the state of the system and must quickly respond to operator commands to set up the state, close adaptive optics control loops, take exposures, etc.

The computer control architecture consists of the basic subsystems shown in Figure XXX.

The AO top level controller that presents the graphical user interface and orchestrates everything (including automated scripts) and commands the bench configuration controller and AO real-time controller. The top level controller also acts to complete the "slow" control loops: e.g. offloading to the telescope tracking, adjusting the first turning mirror to maintain pupil centring, and so on.

The AO optical bench configuration controller maintains motion-controlled items - steering mirrors, dichroic changer, and the like, and speaks the language of the low-level motor controller firmware.

The science camera GUI allows the observer to set up the science instrument and take exposures. The science camera GUI is conceptually separate from the "top level controller" in recognition of the separate roles of the observer from that of the AO operator. There can however be an overlap of functions as appropriate.

The adaptive optics real time controller is a specialized computer designed to respond in real time (1 kHz frame rates) to the wavefront sensor and tip/tilt sensor and to drive the deformable mirrors to track atmospheric turbulence. The RTC interfaces to the top level controller through a socket interface and also provides telemetry data at "human" rates (1-10 Hz) to the displays and writes diagnostic data files as requested.

The top level and science camera control systems

Science Camera GUI

The science camera GUI provides controls for:

1. Setting the science band through filter choice, including blank-off for darks
2. Setting the exposure time
3. Initiating the exposure, allowing for exposure abort
4. Allowing for user-input of FITS header such as object name and comments
5. Recording the science data as FITS files into a secure data base
6. Attaching the FITS headers appropriate for the exposure (see KT Link for a list of FITS header items)
7. All science camera operations are recorded to a text log file, with time stamps

AO System Top Level Control GUI

The AO top level controller provides the information and controls for the AO operator to run the AO system.

The main display allows for the AO and Tip/Tilt loops to be open or closed, and displays the status of these. A graphical display shows the periodic readings from the wavefront sensor (Hartmann slopes and intensities) and the voltages on the deformable mirrors. A button enables Tip/tilt offloading to the telescope guider and shows its status.

Several buttons allow for calibration steps, including taking wavefront sensor darks, flats, reference centroids, and adjusting offsets for image sharpening in closed loop.

All of the operations are scriptable.

All operations steps are recorded to a text log file, with time stamps.

Real-Time Software

This timing-critical component of the AO system requires a processor that is specially designed for to respond to regular interrupts from a master clock derived from the wavefront sensor camera. The Shack-Hartmann sensor and the Tip/Tilt sensor are inputs. These sensors run at independent frame rates, although it is expected that one camera will act as master with the other slaved so as to make the frame rates an integral ratio.

The outputs are two deformable mirrors (DMs): the woofer DM and the tweeter DM. In addition there are a number of ancillary outputs required from the RTC for offloading. The offloading loops are described in the "Slow Loops" section.

In addition to maintaining these fast control loops, the RTC is also required to

1. periodically provide telemetry signals to the top level controller.

2. write diagnostics streams to data files.

The fast loop processing in the RTC consists of:

Path W: WFS to phase:

      W.1 Camera raw data processing

      W.1.1 Frame grab

      W.2.2 Dark subtraction

      W.2.3 Flat-field correction

      W.2 Subaperture definition and data extraction

      W.3 Process subapertures

      W.3.1 Calculate intensities

      W.3.2 Send intensities to low-pass (temporal anti-aliasing) filters

      W.3.3 Calculate centroids (calculate wavefront slopes)

W.4 Reconstruct (calculate phase from slopes)

      W.5 In laser guidestar mode, compute tip/tilt components and subtract them from the reconstructed phase.

      Path T: Tip/Tilt/Focus sensor (TTFS) to low-order components of wavefront (laser guidestar mode only):

      T.1. Camera raw data processing

      T.1.1 Frame grab

      T.1.2 Dark subtraction

      T.1.3 Flat-field correction

      T.2 Region of interest definition

T.2.1 A region of interest will be provided by the target acquisition system

T.2.2 Extract region of interest from raw frame – this is a fixed sized sub field

T.3 Wavefront data extraction

T.3.1 Calculate tip/tilt components

T.3.2 Calculate focus component

T.3.3 Send focus component to its low-pass (temporal anti-aliasing) filter

Path O: Wavefront to Woofer

O.1 If in laser guidestar mode, add phase from path W to the tip/tilt from path T

O.2 Fit phase to the woofer influence functions to determine woofer delta commands

O.3 Woofer processing

O.3.1 Accumulate woofer commands on integrators (the 57 integrators for the woofer are state variables)

O.3.2 Limit the integrator values to the woofer dynamic range limits (clip values in the integrator state variables).

O.3.3 Compute residual due to clipping and subtract from the woofer-fit phase

O.4 Send commands (values in the integrators) to woofer via the woofer driver

O.5 Send integrator values to low-pass (temporal anti-aliasing) filters

Path E: Wavefront minus Woofer-fit to Tweeter

E.1 Subtract the woofer-fit phase from the wavefront phase

E.2 Fit the phase to the tweeter influence functions to determine tweeter delta commands

E.3 Tweeter processing

E.3.1 Accumulate tweeter command on the integrators (the 1020 integrators for the tweeter are state variables)

E.3.2 Limit the integrator values to the tweeter dynamic range limits (clip values in the integrator state variables)

E.4 Send commands (values in the integrators) to the tweeter via the tweeter driver

Path U: Wavefront tip/tilt to laser uplink fast steering mirror (laser guidestar mode only)

U.1 Input delta tip/tilt components from the wavefront sensor processing in path W

U.2 Use the delta tip/tilt as inputs to the uplink control compensator. There are state variables in this compensator.

U.3 Limit the values in the uplink control compensator state variables so as to prevent windup.

A diagram of the real-time AO software flow is shown in Figure 51. A diagram of the real-time controller's loops is shown in Figure 52.
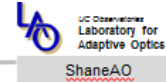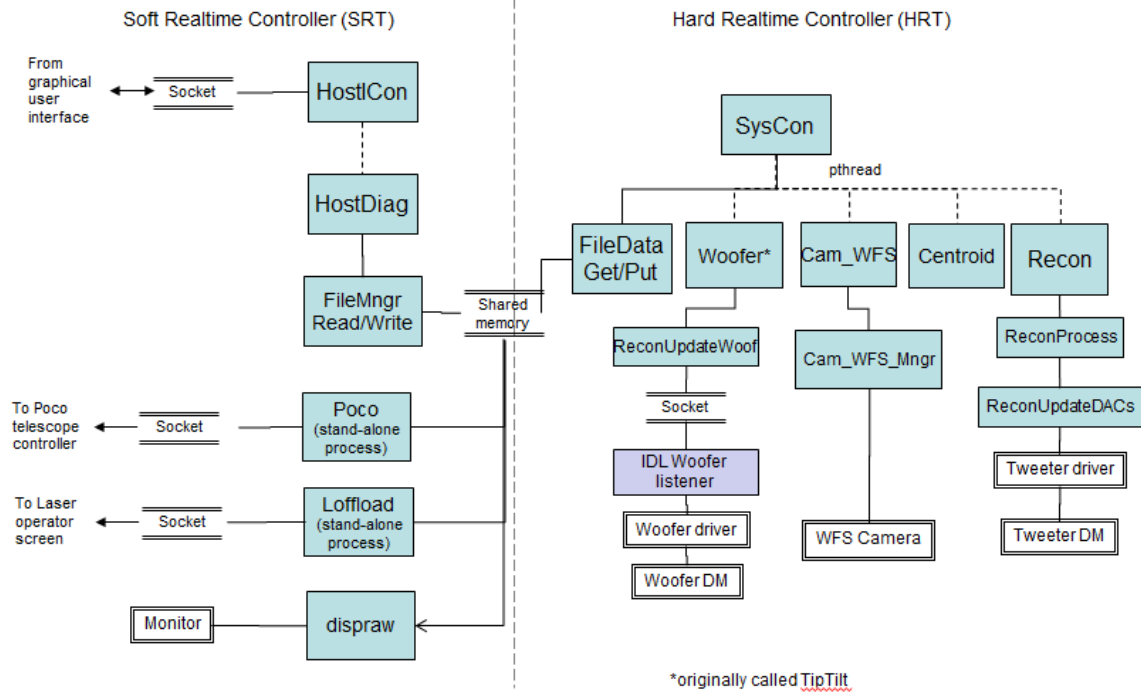
Figure 51. Real-time software and "soft real-time" interface structure
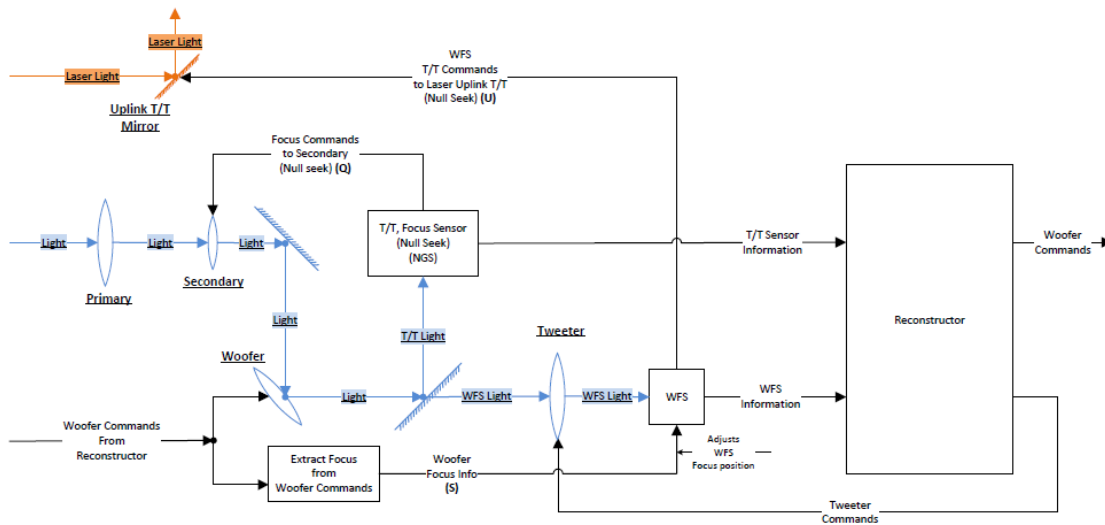

Figure 52. Real-time control loops

Motion Control

Slow Loops

Slow loops are non-time critical yet automated control loops. Using these automated control loops can significantly reduce the burden on the AO system operator from constantly having to monitor several items..

Some of these loops require outputs from the RTC. These signals within the RTC are samples at a very high rate and so need to be low-pass "anti-alias" filtered in the RTC before sending to offloading paths. If this is not possible or desirable in the first version of the RTC, an alternative is to use the diagnostic stream data coming from the RTC, although this is less desirable since it may be aliased.

1. Offloading telescope tracking and focus

   Path F: Offload woofer to telescope

   F.1 Offload to telescope tracking

   F.1.1 Extract tip and tilt components of low-pass filtered woofer phase. Note: these are in actuator space, so a linear transformation is needed to determine the flat component of the mirror shape in phase space.

   F.1.2 Rotate tip and tilt axes to align to telescope RA and Dec axes

   F.1.3 Send offloading command to telescope controller (TELCO)

   F.2 Offload to telescope focus (natural guide star mode only)

   F.2.1 Extract focus components of low-pass filtered woofer phase. Again note: these are in actuator space, so a linear transformation is needed to determine the focus component of the mirror shape in phase space.

   F.2.2 Scale this defocus to a telescope secondary change value

   F.2.3 Send focus change command to the telescope controller (TELCO)

   F.2.4 TELCO should report back its focus stage position. Warn if it is reaching its limit of motion

   Path Q: Offload focus from tip/tilt/focus sensor to telescope (laser guidestar mode only)

   Q.1 Take the low-pass filtered focus as calculated by the TTFS processing on path T

   Q.2 Scale this defocus to a telescope secondary change value

   Q.3 Send focus change command to the telescope controller (TELCO)

   Q.4 TELCO should report back its focus stage position. Warn if it is reaching its limit of motion

1. Autocentering telescope pupil to AO pupil

Path C: Offload centering from wavefront sensor to first turning mirror

   C.1 Take the low-pass filtered subaperture intensities calculated by the WFS processing on path W (W.3.2)

   C.2 Compute the decentering amount from these values, scaled to first turning mirror moves

   C.3 Update position of first turning mirror. The position itself is the state variable.

   C.4 Warn if the turning mirror is reaching its limits of motion.

1. Tracking of the sodium layer distance

   Path S: Offload woofer focus to wavefront sensor stage (laser guidestar mode only)

   S.1 Extract focus components of low-pass filtered woofer phase. Again note: these are in actuator space, so a linear transformation is needed to determine the focus component of the mirror shape in phase space.

   S.2 Calculate the delta position change on the wavefront sensor stage.

   S.3 Update commanded position of the wavefront sensor stage. Note: the stage position itself is the state variable, or integrator, for this control loop.

S.4 Warn if stage is reaching its limit of motion

1. Tip/Tilt star acquisition

Path A: Guider to tip/tilt/focus sensor

A.1 Guider to on-AO bench acquisition ("Flea") camera

A.2 On-AO bench acquisition camera to tip/tilt/focus sensor stage

1.7.12 Electronics

The ShaneAO system has a considerable number of electronics units associated with it. Please refer to the *ShaneAO.xlsx spreadsheet*, "Electronics" tab, for the complete list with relevant details for each item. The design philosophy has been to mount the minimal amount of electronics actually on the telescope, essentially only those that need analog drive signals and therefore require short cable paths to the controlled physical devices on the optics table. Digital control units (right now, essentially just the real-time control computer system) will be mounted off-telescope, with dedicated fiber optic connection handling the digital data traffic to units on-telescope. This approach saves considerable weight and heat load on-telescope.

With this arrangement, the on-telescope units occupy approximately 35 rack units (U) of 19-inch wide rack space. This is handled with custom mini-racks positioned within the frame structure surrounding the optical table. Holes through the table at key places accommodate cable feed-throughs, with the critical length runs being the two deformable mirrors and the two CCD cameras, which all have restricted length multi-conductor cables provided by the manufacturer.

The electronics racks are connected to and transported with the instrument at all stages: when it is moved from prep lab to telescope and when mounted on the telescope. This "tethering" precludes a need to routinely connect / disconnect cables between the bench and electronics rack. Mechanically, the racks are attached to the external frame structure, which is in turn mounted to the telescope.

Motion Control Devices

Motion control consists of

Servo motors for pointing of mirrors

Servo motors for positioning of stages

Piezo drive motors for micro-positioning alignment

The servo motors are used regularly during on-sky observing operations, and the stages they control are load-side encoded. The piezo controlled devices are "set and forget" and used during optical alignment in preparation for an observing run. Please refer to the *ShaneAO.xlsx spreadsheet*, "Controlled Devices" tab for a list of motion-controlled devices and details concerning encoding, precision, motor type, etc.

Servo motors are driven by Galil hardware and standard driver code that is observatory standard. Approximately 12 U of rack space is dedicated to the motion control, drivers, and power supplies, and the associated programmable power strips and fan trays.

Camera Drives, DM Drives, and Other Electronics

Other electronics units consist of

Camera controllers (WFS CCDs and Hi2RG controller)

Deformable mirror controllers

Bus extender with fiber-to-bus conversion – these allow the above controllers to appear on the real-time controller's PCI bus.

Calibration light sources

Ethernet hubs, parallel–to-serial converters

Programmable power strips and fan trays

Approximately 23 U of rack space is associated with these items.

Power and Other On-telescope Infrastructure

120 volt line power is supplied at the telescope hub and feeds the power strips in each electronics rack.

CAT-5 Ethernet is provided at the telescope Cassegrain mount, so the ShaneAO hubs will be connected to it.

Fiber optics cables are supplied through the telescope wraps. Two of these cables will be used to connect the high-speed digital signals from off-telescope electronics to on-telescope electronics.

Heat Management

For heat management, the electronics racks are each enclosed, and define a clear path for air flow past the electronics in each rack mounted unit.

To remove the warm air from the electronics enclosures, we have two options presently being evaluated: 1) ducting the air off-telescope, which would require a wide flexible duct somehow directing air well away from the telescope and optical bench, and 2) using heat exchanger and glycol cooling system. Each of these options has advantages and disadvantages with respect to the present telescope and dome. An air duct system would allow the air-flow fans to be mounted off-telescope, which would minimize coupling vibration to the optical bench. The ducts however would have to be somehow articulated when the telescope is moving so that it does not hang up on other items in the dome. In the case of glycol cooling, the Shane does not presently supply glycol for mounted instruments, so the infrastructure to support this would have to be added. This is a clean option not requiring cumbersome ducting, but will require room in the racks for fans and heat exchangers, and care would have to be taken in the design to prevent coupling of fan vibrations or coolant flow vibrations to the optical bench.

1.8 Bibliographical References

Bogdanovi, T., Ge, J., Max, C. E., & Raschke, L. M. Circumnuclear Shock and Starburst in NGC 6240: Near-Infrared Imaging and Spectroscopy with Adaptive Optics, AJ 126, 2299 (2003)

Burgasser, A. J., Kirkpatrick, J. D., & Lowrance, P. J. Multiplicity among Widely Separated Brown Dwarf Companions to Nearby Stars: Gliese 337CD, AJ 129, 2849 (2005)

Chen, H.-W., Lanzetta, K. M., Webb, J. K., & Barcons, X. The Gaseous Extent of Galaxies and the Origin of Lyα Absorption Systems. V. Optical and Near-Infrared Photometry of Lyα-absorbing Galaxies at z<1, ApJ 559, 654 (2001)

Chun, M. R., Gharanfoli, S., Kulkarni, V. P., & Takamiya, M. Adaptive Optics Imaging of Low-Redshift Damped Lyα Quasar Absorbers, AJ 131, 686 (2006)

Denman, C., J. Drummond, M. Eickhoff, R.Q. Fugate, P. Hillman, S. Novotny, J. Telle, "*Characteristics of sodium guidestars created by the 50-watt FASOR and first closed-loop AO results at the Starfire Optical Range*," **Proceedings of the SPIE** 6272, (2006).

Drummond, J., & Christou, J. Triaxial ellipsoid dimensions and rotational poles of seven asteroids from Lick Observatory adaptive optics images, and of Ceres, Icarus 197, 480 (2008)

Evans, J.W., Morzinski, K., Severson, S., Poyneer, L., Macintosh, B., Dillon, D., Reza, L., Gavel, D., Palmer, D., Olivier, S., Bierden, P, "*Extreme Adaptive Optics Testbed: Performance and Characterization of a 1024-MEMS Deformable Mirror*," **Proceedings of the SPIE**, Volume 6113, (2006).

Ferrarese, L., & Merritt, D. A Fundamental Relation between Supermassive Black Holes and Their Host Galaxies, ApJ 539, L9 (2000)

Gavel, D., and C. Rockosi. *A high-performance adaptive optics system and camera for the Lick Observatory 3-meter telescope.* NSF proposal #0923895, 2009.

Gavel, D., "MEMS Development for Astronomical Instrumentation at the Lick Observatory Laboratory for Adaptive Optics," **Proceedings of the SPIE**, Vol. 6467, (2007).

Gavel, D., Ammons, M., Bauman, B., Dillon, D., Gates, E., Grigsby, B., Johnson, J., Lockwood, C., Morzinski, K., Palmer, D., Reinig, M., Severson, S., "*Visible light laser guidestar experimental system (Villages): on-sky tests of new technologies for visible wavelength all-sky coverage adaptive optics systems*," **Proc. SPIE Astronomical Telescopes and Instrumentation**, Vol. 7015, (2008).

Gavel, Donald T., Scot S. Olivier, Brian J. Bauman, Claire E. Max and Bruce A. Macintosh, "Progress with the Lick adaptive optics system", Proc. SPIE 4007, 63 (2000);'*http://dx.doi.org/10.1117/12.390289* <http://link.aip.org/link/doi/10.1117/12.390289>'__

Gavel, D.T., J. R. Morris, and R. G. Vernon, "*Systematic Design and Analysis of Laser-Guide-Star Adaptive-Optics Systems for Large Telescopes*," **Journal of the Optical Society of America A**, Vol. 11, No. 2, pp914-924, (1994).

Gebhardt, K., Bender, R., Bower, G., Dressler, A., Faber, S. M., Filippenko, A. V., Green, R., Grillmair, C., Ho, L. C., Kormendy, J., Lauer, T. R., Magorrian, J., Pinkney, J., Richstone, D., & Tremaine, S. A Relationship between Nuclear Black Hole Mass and Galaxy Velocity Dispersion, ApJ 539, L13 (2000)

Goldman, B., Bouy, H., Zapatero Osorio, M. R., Stumpf, M. B., Brandner, W., & Henning, T. Binarity at the L/T brown dwarf transition. Adaptive optics search for companions, A&A 490, 763 (2008)

Johnson, Luke C., Donald T. Gavel and Donald M. Wiberg, "Online wind estimation and prediction for a two-layer frozen flow atmosphere", Proc. SPIE 7736, 77362R (2010); *http://dx.doi.org/10.1117/12.857704*

Kulkarni, V. P., Fall, S. M., Lauroesch, J. T., York, D. G., Welty, D. E., Khare, P., & Truran, J. W. Hubble Space Telescope Observations of Element Abundances in Low-Redshift Damped Ly alpha; Galaxies and Implications for the Global Metallicity-Redshift Relation, ApJ 618, 68 (2005)

Laag, E. A., Canalizo, G., van Breugel, W., Gates, E. L., de Vries, W., & Stanford, S. A. Adaptive Optics Imaging Survey of Luminous Infrared Galaxies, AJ 131, 2877 (2006)

Laag, E., S.M. Ammons, D.T. Gavel, R. Kupke, "*Multi-conjugate adaptive optics results from the laboratory for adaptive optics MCAO/MOAO testbed*," **Journal of the Optical Society of America A**, Vol. 25 Issue 8, pp.2114-2121 (2008).

Lacy, M., Gates, E. L., Ridgway, S. E., de Vries, W., Canalizo, G., Lloyd, J. P., & Graham, J. R. Observations of Quasar Hosts with Adaptive Optics at Lick Observatory, AJ 124, 3023 (2002)

Lacy, M., Sajina, A., Gates, E., & the XFLS team Radio galaxies and type-2 quasars in the Spitzer Extragalactic First Look Survey, AN 327, 258 (2006)

Lepine, S., Rich, R. M., Shara, M. M., Cruz, K. L., & Skemer, A. An Astrometric Companion to the Nearby Metal-Poor, Low-Mass Star LHS 1589, ApJ 668, 507 (2007)

Marchis, F., Descamps, P., Hestroffer, D., Berthier, J., Vachier, F., Boccaletti, A., de Pater, I., & Gavel, D. A three-dimensional solution for the orbit of the asteroidal satellite of 22 Kalliope, Icarus 165, 112 (2003)

Marcy, G. W., Butler, R. P., Vogt, S. S., Liu, M. C., Laughlin, G., Apps, K., Graham, J. R., Lloyd, J., Luhman, K. L., & Jayawardhana, R. Two Substellar Companions Orbiting HD 168443, ApJ 555, 418 (2001)

Max, C.E., S.S. Olivier, H.W. Friedman, J. An, K. Avicola, B.V. Beeman, H.D. Bissinger, J.M. Brase, G.V. Erbert, D.T. Gavel, K. Kanz, B. Macintosh, K.P. Neeb, K.E. Waltjen, M.C. Liu, and J. Patience, "Image improvement from a sodium-layer laser guide star adaptive optics system," **Science**, 277, pp 1649-1652, September 12, 1997.

Patience, J., White, R. J., Ghez, A. M., McCabe, C., McLean, I. S., Larkin, J. E., Prato, L., Kim, S. S., Lloyd, J. P., Liu, M. C., Graham, J. R., Macintosh, B. A., Gavel, D. T., Max, C. E., Bauman, B. J., Olivier, S. S., Wizinowich, P., & Acton, D. S. Stellar Companions to Stars with Planets, ApJ 581, 654 (2002)

Perrin, M. D., Graham, J. R., & Lloyd, J. P. The IRCAL Polarimeter: Design, Calibration, and Data Reduction for an Adaptive Optics Imaging Polarimeter, PASP 120, 555 (2008)

Roe, H. G., Gavel, D., Max, C., de Pater, I., Gibbard, S., Macintosh, B., & Baines, K. H. Near-Infrared Observations of Neptune's Tropospheric Cloud Layer with the Lick Observatory Adaptive Optics System, AJ 122, 1636 (2001)

INDICES AND TABLES

- genindex
- search